JPL PUBLICATION 80-93

NASA-CR-164077
19810011811

The Deep Space Network – An Instrument for Radio Science Research

N.A. Renzetti
A.L. Berman

February 15, 1981

National Aeronautics and
Space Administration

Jet Propulsion Laboratory
California Institute of Technology
Pasadena, California

JPL PUBLICATION 80-93

The Deep Space Network - An Instrument for Radio Science Research

N.A. Renzetti
A.L. Berman

February 15, 1981

National Aeronautics and
Space Administration

Jet Propulsion Laboratory
California Institute of Technology
Pasadena, California

The research described in this publication was carried out by the Jet Propulsion Laboratory, California Institute of Technology, under contract with the National Aeronautics and Space Administration.

ACKNOWLEDGMENTS

The authors would like to thank J. D. Anderson, B. J. Buckles, R. C. Chandlee, W. D. Chaney, R. M. Goldstein, A. J. Kliore, G. S. Levy, B. Seidel, G. L. Spradlin, C. T. Stelzried, and J. A. Wackley, all of the Jet Propulsion Laboratory, for many excellent comments and suggestions.

ABSTRACT

Doppler and ranging data routinely generated at the Deep Space Stations of the California Institute of Technology-Jet Propulsion Laboratory Deep Space Network serve as an excellent source of radio science information. Important radio science experiments based on Deep Space Network generated radio metric data have included confirmation of Einstein's Theory of Relativity, measurement of the masses and grativational harmonics of the planets out to Saturn, and measurement of electron density distribution and turbulence in the solar corona.

In response to an increased level of radio science requirements, the Deep Space Network chose in 1976 to implement a new radio science system, which was subsequently completed in late 1978. Key features of this new system include (1) highly phase-stable open loop receivers, (2) reduction of recorded data bandwidth through use of programmed local oscillators, and (3) real-time digitization and recording on computer compatible tape.

The major radio science system challenge of the 1980s will be the proposed upgrading of the entire signal path to a fractional frequency fluctuation of 10^{-15} over time scales between 50 and 5000 seconds, enabling the important search for gravitational waves. To achieve this capability, the Deep Space Network will have to operate both spacecraft-ground links ("uplink" and "downlink") at X-band ($\sim$ 8.4 GHz) or higher frequencies.

TABLE OF CONTENTS

TABLES

FIGURES

I. INTRODUCTION

The Deep Space Network (DSN), managed by The California Institute of Technology-Jet Propulsion Laboratory for the U.S. National Aeronautics and Space Administration, is the organization which communicates with, controls, navigates, and collects data from spacecraft involved in the exploration of our Solar System. The DSN in 1981 includes major Deep Space Station complexes located approximately 120 degrees around the Earth at Goldstone, California; Madrid, Spain; and Canberra, Australia. These stations are connected to a central Mission Control Center located in Pasadena via a world-wide ground communications facility. Each Deep Space Station (DSS) complex contains one 64-m diameter antenna, one 34-m diameter antenna, and one or more 26-m diameter antennas. The DSSs are characterized by high-power transmitters, low-noise microwave amplifiers, phase-locked loop receiving systems, and multiple digital data handling subsystems controlled by minicomputers.

Organizationally, the Deep Space Network is composed of 9 major data oriented systems:

Tracking
Telemetry
Command
Monitor & Control
Test Support
Programming
Radio Science
Very Long Baseline Interferometry
Frequency and Timing

Of major interest to the generation of radio science data are two of the above systems: The Tracking System, which generates radio metric data such as spacecraft angles, doppler (accumulated signal phase), and range (signal time delay), and the Radio Science System, which generates baseband digitized amplitude samples of the spacecraft carrier signal. The Radio Science System is a rather recent addition to the DSN (Berman

and Ramos, 1980), while the Tracking System dates back to the inception of the first Deep Space Station in the late 1950s (DSS 11 at Goldstone in 1958). Since most of the early radio science data were generated through the Tracking System (augmented in some cases with open-loop receivers), it serves as the initial focus of this report.

II. THE DSN TRACKING SYSTEM

The Tracking System in overview provides a two-way "coherent" communications link with the spacecraft, which enables commanding of the spacecraft, reception of spacecraft telemetry data, and generation of both spacecraft navigational and radio science data. Figure 1 (Spradlin, 1980) presents a simplified block diagram of the Tracking System. One begins with the Frequency and Timing Subsystem (FTS), which generates and provides to the Exciter Assembly an ultrastable frequency reference. The Exciter Assembly in turn provides a carrier frequency (S-band) signal to the Transmitter Subsystem. The FTS utilizes Rubidium and Cesium Frequency Standards, and more recently, Hydrogen Masers. The fractional frequency stability performance in the low-frequency regime (approximately 10^{-1} to 10^{-3} Hz) of the Rubidium Standard is 10^{-12}, the Cesium Standard 10^{-13}, and the Hydrogen Maser, better than 10^{-14}.

Depending on the particular receiver-exciter, the FTS provides either a 5 MHz or 50 MHz reference to the Exciter Assembly. Here the signal is multiplied up to S-band ($\sim$2.1 GHz) and binary coded ranging modulation from the Planetary Ranging Assembly is applied. Next, the Transmitter Subsystem, utilizing a klystron power amplifier, increases the signal power from the several watts level to approximately 20 kW. The Antenna Microwave Subsystem illuminates the antenna surface with the signal, which is then radiated toward the spacecraft following signal collection and focusing by the Antenna Mechanical Subsystem. The spacecraft receives the signal, coherently multiplies it (by 240/221) to a slightly different S-band frequency ($\sim$2.3 GHz) so as to avoid potential interference in the Antenna Microwave Subsystem, and retransmits it back to earth. In some cases, the spacecraft also multiplies the signal by 880/221 to provide an X-band carrier frequency, and simultaneously retransmits this signal to Earth.

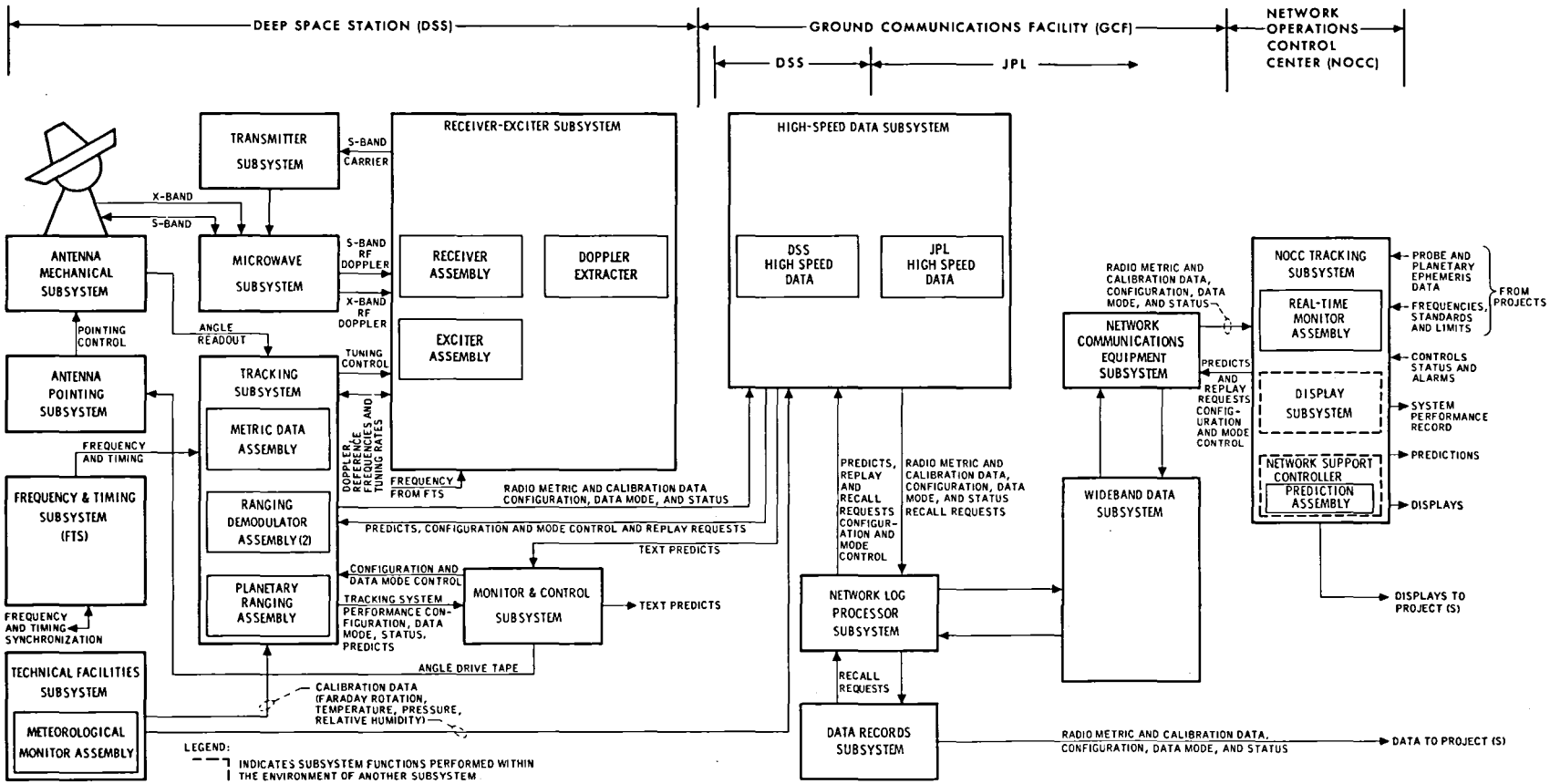

Figure 1. DSN Tracking System (64-m antenna)

After reception on Earth, low-noise amplification of the signal is performed by the Antenna Microwave Subsystem Traveling Wave Maser Amplifier. The system noise temperature at the output of these cryogenically cooled devices is approximately 20 K.

In the receiver, the signal is "tracked" via a phase-locked loop voltage-controlled oscillator (VCO). The output of the phase-locked loop VCO is provided to the Doppler Extractor Assembly, where it is heterodyned with an appropriately multiplied (x240/221) S-band signal provided by the Exciter Assembly, hence closing the tracking loop and thereby providing a coherent two-way system. Finally, the extracted spacecraft doppler is provided to the Tracking Subsystem where it is counted and recorded at the desired sample rate. Also in the Tracking Subsystem, the Planetary Ranging Assembly compares the transmitted range code to the received range code, thus providing discrete estimates of the spacecraft range.

Time-tagged doppler and ranging data are provided in digital form on computer compatible magnetic tape to radio science experimentors. Doppler accuracy for averaging times of 1000 seconds is 0.1 mm/sec; ranging accuracy is 6.0 m for two-station comparisons.

The radio science applications of the Tracking System are numerous. Doppler data provide celestial mechanics information, i.e. mass, gravitational harmonics, etc. for planetary flybys and orbiters, and planetary atmospheric information as the signal is refracted during passage through planetary neutral atmospheres. Additionally, dual-frequency doppler (i.e., two simultaneous and coherent spacecraft-ground links at separate frequencies) provides measurement of columnar electron density changes in the solar wind and planetary ionospheres. Ranging data can be used to measure planetary distances as well as signal retardation due to both solar wind (electron density) and near-sun gravitational (relativistic) bending.

III. SOLAR CORONA AND SOLAR WIND RESEARCH

The first use of the DSN in solar coronal research consisted of a spectral broadening experiment performed by Goldstein et al. (1967) as the Mariner IV (Mars) signal passed within 0.6 deg of the solar disk. Goldstein and colleagues used the not yet completed Goldstone 64-m station (DSS 14) to receive the very weak Mariner IV signals (so weak because the spacecraft antenna was not pointed at Earth). The uplink, provided by a 26-m antenna (DSS 13) was 100 kW, while the 64-m receiving station utilized an open-loop receiver driven by an oscillator programmed with the predicted spacecraft received frequency profile. The radially dependent spectral broadening obtained by Goldstein and colleagues reflected the now better understood relationship between spectral broadening and integrated coronal electron density (Woo, 1978; Berman, 1978a, 1979a). These historic data are reproduced in Figure 2. In 1968, Goldstein (1969) duplicated the experiment with the superior conjunction of the Pioneer 6 Spacecraft, and obtained results similar to those previously obtained during the Mariner IV experiment.

More recently, Woo (1978) has obtained extensive near-sun spectral broadening measurements of the Helios 1 and 2 spacecrafts, and has used these data in a theoretical examination of spectral broadening. Figure 3 (Rockwell, 1978) presents a substantial set of Helios and Pioneer spectral broadening data, which have been empirically compared to an integrated electron density (N_e) model of the form:

$$N_e = Ar^{-6} + Br^{-2.3}$$

where:

r = radial distance

A, B = fit constants

In November 1968, the Pioneer VI spacecraft was occulted by the Sun. Pioneer VI transmitted a linear polarized carrier, which allowed the first

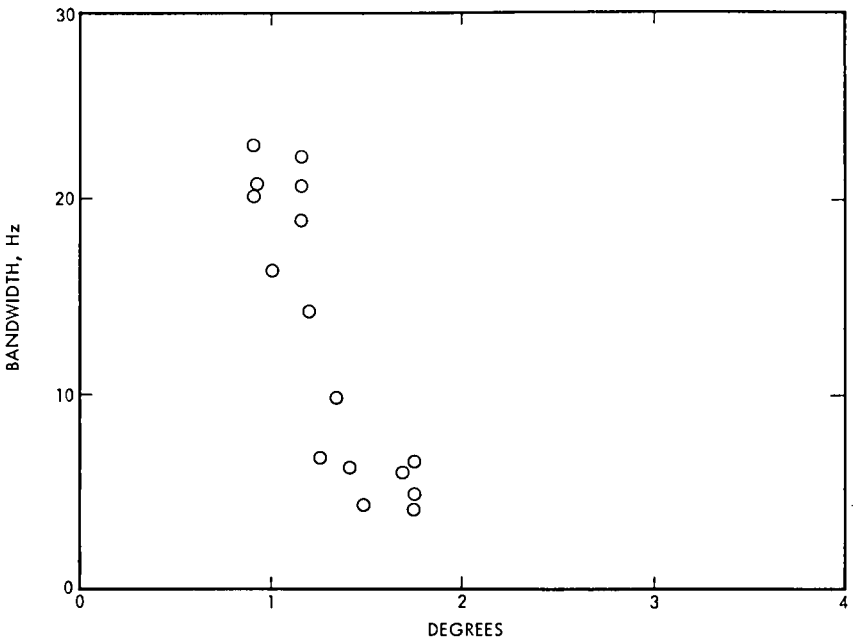

Figure 2. Mariner IV Spectral Broadening Data

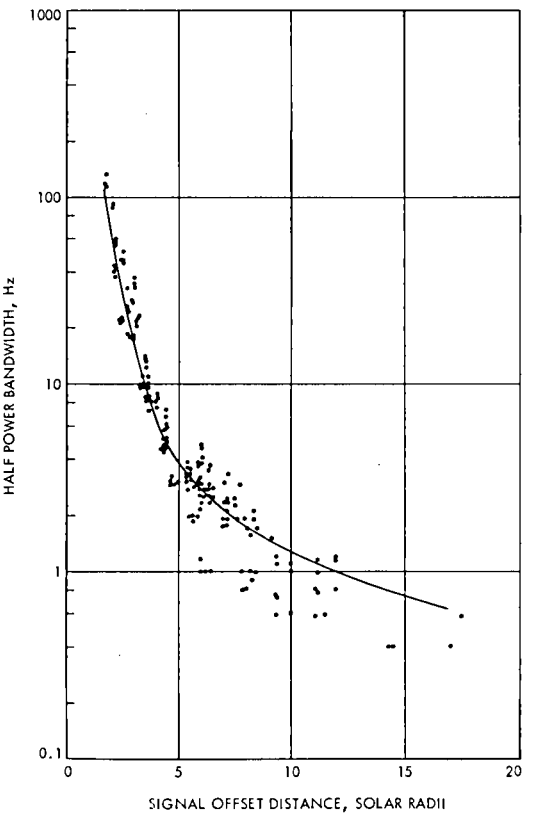

Figure 3. Spectral Broadening Data Versus Signal Offset Distance

experiment to be performed using a man-made signal source in determining Faraday rotation through the solar corona (Stelzried, 1970). The quasi-longitudinal approximation for Faraday rotation is given by (Stelzried et al., 1970):

$$\Omega = Qf^{-2} \int N_e B_l dR$$

where:

Ω = Faraday rotation, deg
f = signal carrier frequency, Hz
Q = 1.3548×10^6
R = signal path, m
N_e = electron density, m^{-3}
B_l = solar longitudinal component of magnetic field, tesla

Therefore, measurement of coronal induced Faraday rotation provides information about both electron density and the solar magnetic field (Rusch and Stelzried, 1972). To support this experiment, DSS 14 was equipped with a remotely rotatable, microwave linear feed (Reid et al., 1973). A closed-loop polarimeter (Ohlson et al., 1974) was implemented and used to automatically track the orientation of the received signal polarization. This system maximized the received signal strength and yielded precise signal polarization data. Observations during November-December 1968 yielded information on both solar coronal transient events (Levy et al., 1969), and the steady state solar corona. Research using the polarization tracking capability at DSS 14, 43, and 63 has continued with Pioneer and Helios spacecraft; recently Volland et al. (1977) and Bird et al. (1977) have reported Faraday rotation observations from the solar occultations of Helios 1 in 1975. Dennison et al. (1978) have expanded on these results with a measurement of the gravitational deflection of polarized signal radiation propagating through the solar corona.

The effect of columnar charged particles on the group velocity of electromagnetic waves is given by Koehler (1968) as

$$r = Kf^{-2}\int N_e dR$$

where:

r = observed range delay, m
K = 40.3
f = carrier frequency, Hz
N_e = electron density, m^{-3}
R = signal path, m

For spacecrafts in solar conjunction phases, range measurements as a function of solar offset distance provide an excellent method of mapping electron density in the solar corona, provided all other competing effects, such as trajectory errors, unmodelled spacecraft forces, relativistic effects, etc., can be properly accounted for. Muhleman et al. (1971) first used this method during the solar conjunctions of Mariners 6 and 7. Using ranging data acquired at DSS 14, Muhleman and colleagues (Muhleman et al., 1977) were able to model the coronal electron density as:

$$N_e = Ar^{-6} + Br^{-\varepsilon}$$

ε = 2.05 (Mariner-6)
2.08 (Mariner-7)

a functional form which is in good agreement with earlier eclipse measurements.

A far more powerful tool for measuring electron density is available when dual-frequency carriers are transmitted from a spacecraft. In this case, differenced range measurements made at the two frequencies provide a

direct measurement of columnar electron density, and such measurements are not contaminated with the multitude of other factors previously mentioned. The Viking Spacecraft were equipped with dual-frequency capability, and the 1976-77 and 1978-79 Viking solar conjunctions provided excellent electron density measurements. A set of these data (Berman, 1979b) is illustrated in Figure 4.

Using single frequency (S-band) doppler data during the 1975 solar conjunctions of Pioneer 10, Pioneer 11, and Helios 1, Berman and Wackley (1976) demonstrated that the observed doppler fluctuations provide an excellent measure of solar wind turbulence. This was significant in that doppler fluctuation was already being automatically computed for purposes of ground tracking system performance monitoring, and hence represented a "free" source of coronal scientific data. Using this data type, it was demonstrated (Berman et al., 1981) that columnar turbulence is proportional to integrated electron density. Figure 5 presents concurrent measurements of Viking doppler noise and integrated electron content derived from dual-frequency ranging measurements.

Utilizing dual-frequency (S-band minus X-band) doppler data from the Mariner 10 spacecraft, Woo et al. (1977) were able to demonstrate that the columnar phase fluctuation spectral index was approximately -2.6:

$$W_o(\nu) \propto \nu^{-2.6}$$

where:

W_o = columnar phase spectral density, rad^2/Hz

ν = fluctuation frequency, Hz

The work of Woo et al. made a significant contribution to the gradual resolution of a controversy about the value of the spectral index which originated in the early days of (natural source) interplanetary scintillation study (early 1970s). More recently, Woo and Armstrong (1979) have studied the variation of the spectral index with radial

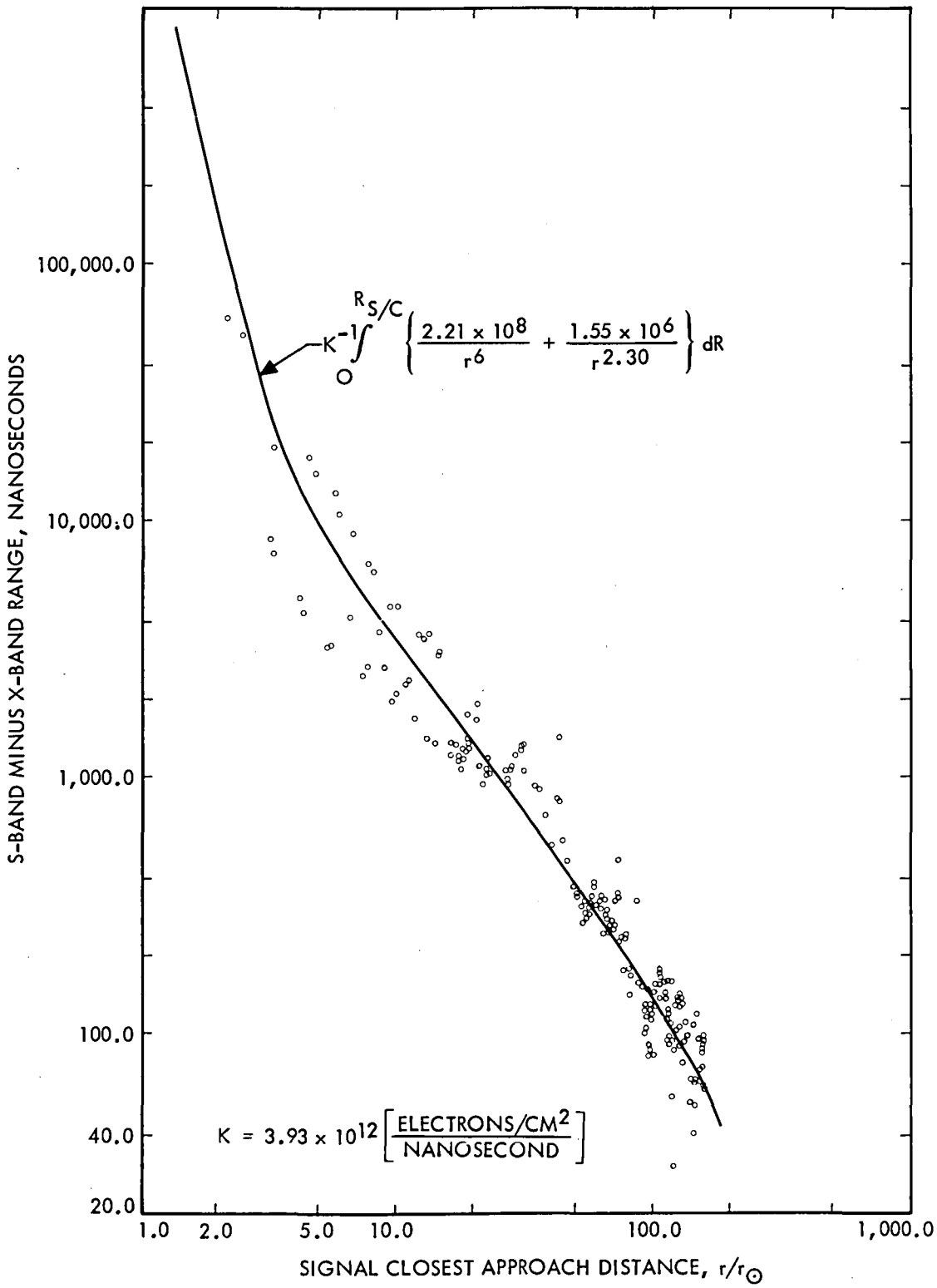

Figure 4. Viking Columnar Electron Density Measurements

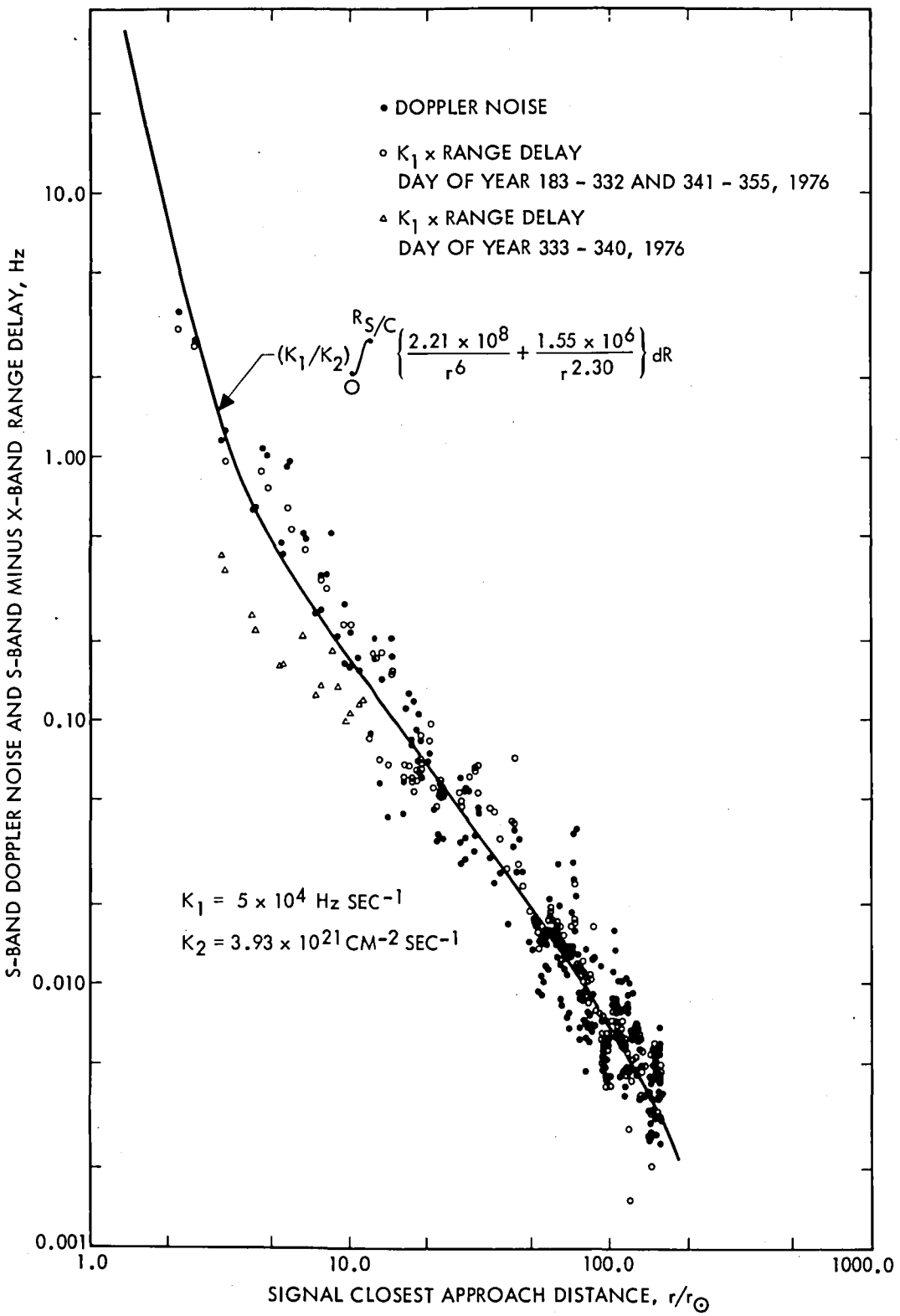

Figure 5. Concurrent Measurements of Viking 2.3 GHz Signal Frequency Fluctuation and Columnar Electron Density

distance (using Viking solar conjunction data) and have concluded that a significant change exists in the spectral index at a solar offset distance of approximately 20 solar radii. Figure 6 presents a phase fluctuation spectrum generated from dual-frequency Mariner 10 data.

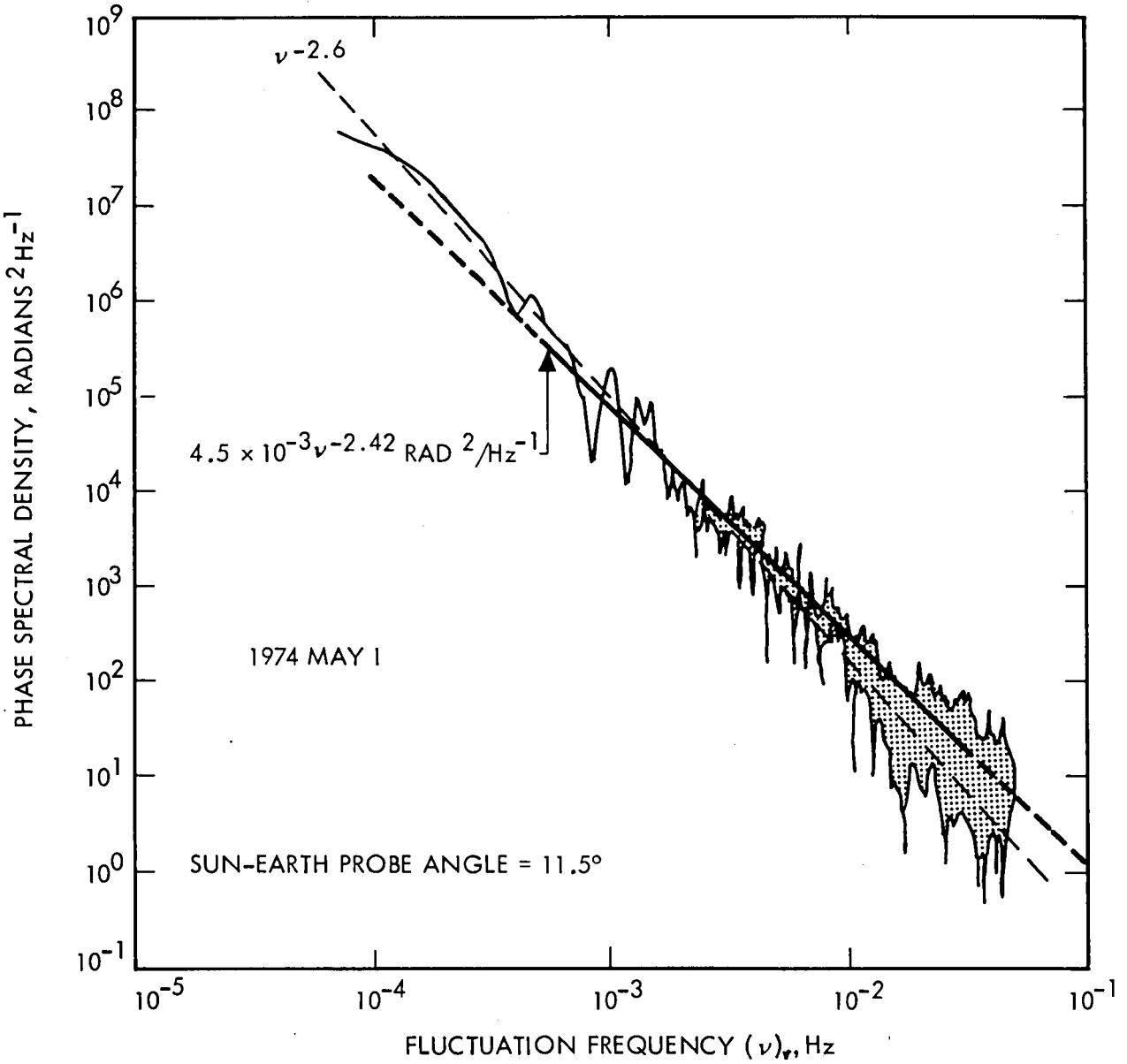

Figure 6. Mariner 10 Phase Spectral Density

IV. MEASUREMENTS OF RELATIVISTIC TIME DELAY

One of the most exciting aspects of the capability to obtain range measurements from spacecrafts in solar conjunction phases is the ability to test that portion of Einstein's Theory of Relativity that predicts that electromagnetic waves passing close to a massive body (e.g., the sun) are "bent" by the intense gravitational force. The "bending" appears as a signal time delay, which is dependent upon the observer-sun-spacecraft geometry as follows:

$$\Delta t = 2GM_o c^{-3}(1 + \gamma)\ln((r_e + r_m + R)(r_e + r_m - R)^{-1})$$

where:

Δt = signal delay, sec
GM_o = Solar mass, km^3/sec^2
c = speed of light, km/sec
r_e = earth-sun distance, km
r_m = sun-spacecraft distance, km
R = earth-spacecraft distance, km
γ = generalized Schwarzschild metric

In Einstein's Theory of General Relativity, γ is replaced by 1. Hence the nature of the experiment is to verify that γ indeed equals 1.

To measure signal time delay the DSN utilizes a binary coded sequential-acquisition ranging system, of which the primary dedicated hardware is referred to as the Planetary Ranging Assembly. Figure 7 presents a simplified block diagram of this system (Tappan, 1974). A frequency synthesizer, which is controlled by the Hydrogen Maser Frequency Standard, generates a 22 MHz reference which is multiplied by 3 and phase modulated by a transmitter coder. The ranging code is generated by dividing the 66 MHz frequency by 64 and applying the resultant frequency

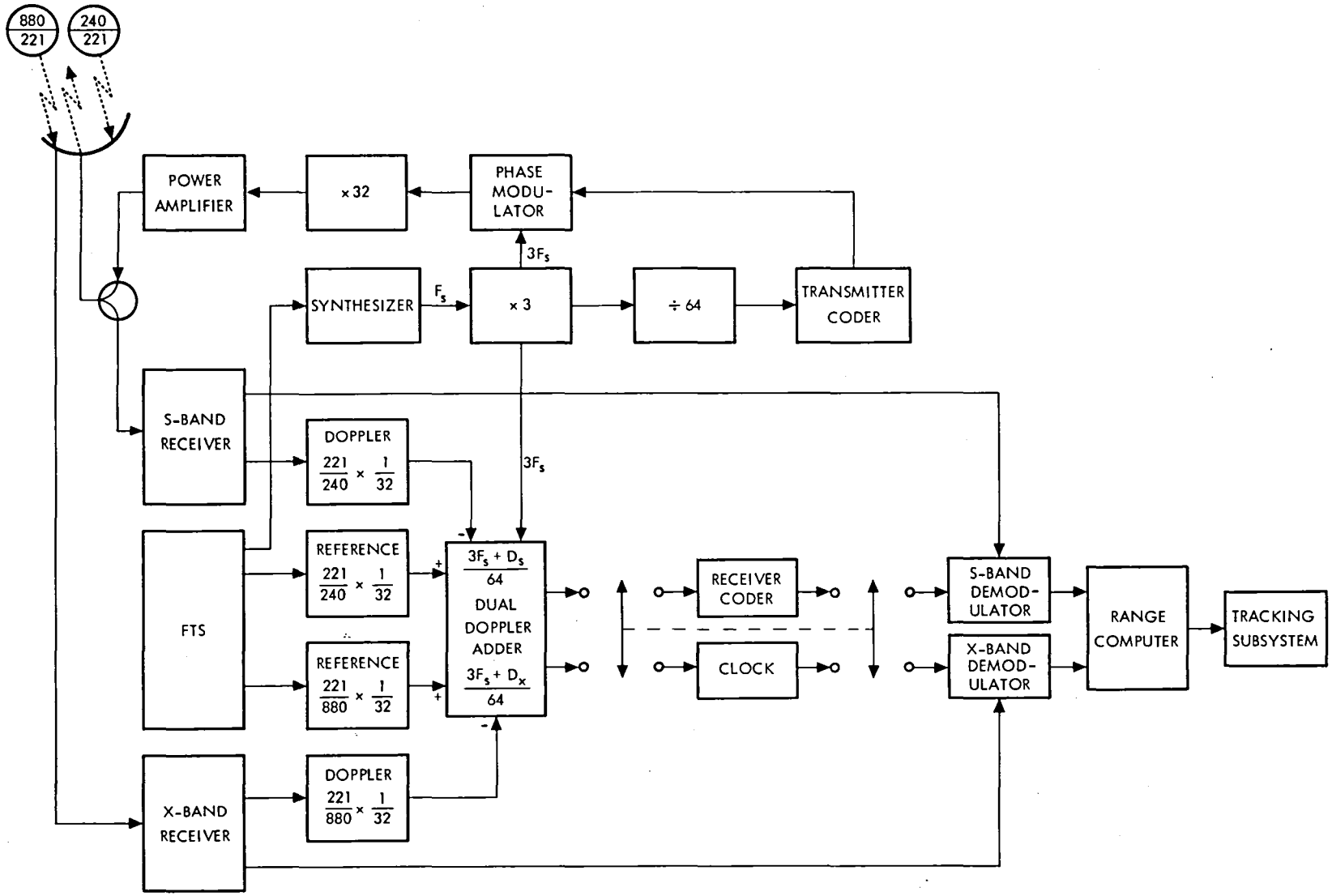

Figure 7. Planetary Ranging Assembly Block Diagram

to an 18 stage binary counter, whose outputs are singly selectable for transmitter modulation. The periods of the resultant codes are:

$$t_m = 2^{6+m}(66 \times 10^6 \text{Hz})^{-1} \qquad 1 \leq m \leq 18$$

The shortest ("clock") code length is 1 microsecond; it is this code component that determines the basic ranging system resolution, which is approximately at the meter level. Higher codes for resolving the ambiguity in the ranging measurement are selected as needed, depending on the accuracy of the available navigational estimates of the (time-dependent) spacecraft range.

The phase modulated 66 MHz frequency is multiplied by 32 to S-band level, amplified, and transmitted to the spacecraft. At the spacecraft, the ranging code is stripped off. The signal is then multiplied by 240/221 (880/221 for an X-band downlink), remodulated with the ranging code, and retransmitted to the observing DSS.

On the ground, the modulated signal is received and divided down to the 66 MHz level by application of 221/240 (880/221 for X-band) and 1/32 multipliers. At this point the signal could be compared to the transmitted signal, except that it has been further modulated by doppler. To properly account for the doppler modulation, the extracted doppler is added to the transmitter reference. The received signal now can be compared to the coherent transmitted signal, and through correlation of the received signal and the doppler modified transmitted signal, the desired range delay is obtained.

The first major attempt to measure the relativistic bending of a spacecraft signal occurred during the solar conjunctions of Mariner 6 and 7 during mid-1970 (Anderson et al., 1975). This experiment was able to verify the value of γ to about 6%, i.e., $\gamma = 1.00 \pm 0.06$. The major error source that prevented this experiment from achieving greater accuracy was the nongravitational forces on the spacecraft, which limited the accuracy of the orbit determination. Additionally, uncertainties in the signal delay caused by scattering of free electrons in the solar

corona contributed an error of about 2% to the determination of γ from Mariner 6 and 7. Later, the nongravitational noise source was eliminated by the Mariner 9 Mars Orbiter, and a measurement of γ to the 2% level was achieved (Anderson et al., 1978; Reasenberg and Shapiro, 1977).

During 1976-1977, the relativistic experiment was performed using both the Viking Mars Orbiter and Lander Spacecraft (Shapiro et al., 1977; Cain et al., 1978; Reasenberg et al., 1979). Three factors led to a very significant accuracy improvement over the earlier Mariner experiments:

1) Significant improvements were made in the ground equipment; in particular, in the ability to calibrate the ground system ranging delay.

2) The availability of a landed spacecraft. The highly precise knowledge of the landed spacecraft eliminated the much larger positional errors of heliocentric spacecraft, such as those due to orbital errors, unmodelled forces, etc.

3) Dual-frequency downlink (S- and X-band) capability. The dual-frequency downlink capability on the orbital spacecraft permitted accurate measurements of the signal delay due to electron density, thus significantly reducing the plasma uncertainty, which had previously been the largest error source.

Independent determination of the relativity parameter γ at the Jet Propulsion Laboratory and the Massachusetts Institute of Technology led to a value of 1 ± 0.002, which provides a test of general relativity to 0.1%, the most accurate test of the theory to date.

V. CELESTIAL MECHANICS

Perhaps the earliest radio science application of DSN capabilities occurred in the area of celestial mechanics. Previous to the era of deep space exploration, calculation of the physical properties of the planets (mass, size, shape, orbit, etc.) had to be conducted via the standard (optical) astronomical techniques. Obviously, the ability to make accurate distance and velocity measurements to a deep space probe which flew by and was within the gravitational field of a planet represented a quantum step in the ability to accurately determine the physical properties of the planets. Such efforts were initiated with the 1962 Mariner II mission to Venus. Using the doppler navigational data from this flight, Anderson and Warner (1966) were able to make order of magnitude improvements in the determination of the masses of the moon and Venus. Subsequently, Mariner IV (Mars), V (Venus), and Mariner 9 (Mars) provided the mass and gravitational harmonics for Venus and Mars respectively (see Anderson, 1974, for a review).

Analysis of doppler measurements from the Lunar Orbiter and Apollo missions led to the discovery of large positive gravity anomalies ("mas-cons", for mass concentration) on the moon (Sjogren et al., 1976), and the analysis of data from Mariner 10 yielded the mass and dynamical oblateness of Mercury (Esposito et al., 1978; Howard et al., 1974a). More recently, the Pioneer and Voyager missions to the outer planets are yielding a wealth of new and significantly more accurate physical information on Jupiter (Null et al., 1975, Null 1976), the Galilean satellites (Hubbard and Anderson, 1978) and Saturn (Anderson et al., 1980). It is noteworthy that over this 18-year period (1962-1980), the basic ground system doppler accuracy has improved 50-fold, from 5 mm/sec in 1962 to 0.1 mm/sec in 1980.

VI. OCCULTATION EXPERIMENTS

In the early 1960s, D. L. Cain and colleagues at JPL conducted a study of the effect of refraction in the Earth's atmosphere on the accuracy of the counted doppler data generated from spacecraft. In the course of analyzing these effects, they also saw the possibility of applying the remarkable sensitivity of doppler phase measurements to the study of the atmospheres and ionospheres of other planets (Kliore, Cain, and Hamilton, 1964). Simultaneously, this same technique was also developed by Fjeldbo (1964) at Stanford University. The technique involves obtaining a refractivity profile through the ionosphere and neutral atmosphere after navigation has established the best (geometrical) flight path during the period when the spacecraft signal passed through the planetary ionosphere and neutral atmosphere. After obtaining the refractivity profile, it is a rather straightforward conversion to electron density in the ionosphere and pressure and temperature profiles in the neutral atmosphere (Kliore, 1972a).

The equipment required for the occultation experiment was essentially the normal configuration of the DSS doppler system, with the exception of the receiver. The normal ground tracking system receivers employ a phase-locked loop and hence are vulnerable to losses of lock during the occultation period. Valuable data would be lost during subsequent attempts to relock the receivers. Hence, for the occultation experiment, open-loop receivers were installed and used, in addition to the normal usage of closed-loop receivers. The open-loop output was recorded on analog magnetic tape recorders at the DSS. These tapes were then shipped to JPL where they were digitized and thence provided to the experimentors.

The first occultation experiment was performed in 1965 during the Mariner IV mission to Mars (Kliore et al., 1965, Fjeldbo and Eshleman, 1968). This experiment provided the first measurement of the Martian surface pressure and temperature, as well as a measurement of electron density in the Martian ionosphere.

Venus was the next planet probed via occultation experimentation, during the 1967 Mariner V mission (Kliore et al., 1967; Fjeldbo, Kliore, and Eshleman, 1971). Here too, interesting new information was obtained in the pressure and temperature profiles in the neutral Venusian atmosphere and electron density distribution in the Venusian ionosphere, including the fact that the Soviet Venera 4 spacecraft did not reach the surface (Kliore and Cain, 1968; Eshleman et al., 1968).

During the late 1960s and early 1970s, the inner planets continued to be probed via occultation techniques; included were the Mariner 6 and 7 flybys of Mars (Kliore et al., 1969), the Mariner 9 Orbiter (Kliore et al., 1972b; Kliore et al., 1973), and the Mariner 10 flybys of Venus (Howard et al., 1974b; Kliore et al., 1979a) and Mercury (Howard et al., 1974a; Fjeldbo et al., 1976).

The two Viking Orbiters and Landers provided large amounts of important occultation data during a mission to Mars which began in 1976 and is still continuing (Fjeldbo et al., 1977; Lindal et al., 1979).

In 1973, the Pioneer 10 spacecraft passed by Jupiter, allowing the first occultation probing of an outer planet. Analysis of these data disclosed the existence of an atmosphere on Io (Kliore and Woiceshyn, 1976; Kliore et al., 1975). Measurements of the Jovian ionosphere were also obtained (Fjeldbo et al., 1975). In 1974, Jupiter was again probed by the Pioneer 11 spacecraft, and in 1979 by the Voyager 1 and 2 spacecraft (Eshleman et al., 1979a,b). Very recently, an occultation experiment was performed during the Pioneer 11 encounter of Saturn, and this experiment has yielded the first accurate measurements at the atmosphere and ionosphere of Saturn (Kliore et al., 1980a; 1980b).

Since December 1979, the Pioneer Venus spacecraft has been orbiting Venus and providing important data on the structure of the ionosphere (Kliore et al., 1979b,c) and atmosphere (Kliore and Patel, 1980; Cimino et al., 1980; Woo et al., 1980).

VII. THE DSN RADIO SCIENCE SYSTEM

Early (circa 1976) in the planning for the Pioneer Venus Orbiter Mission, it became obvious that the DSN and experimenter data handling and processing would be exceedingly costly with the then existing analog occultation system. The baseband frequency bandwidths which would need to be recorded to accommodate the doppler frequency shifts, orbital uncertainities, and spacecraft transmission frequency uncertainties were on the order of 100 kHz for S-band and 300 kHz for X-band. The combined S- and X-band bandwidth of 400 kHz would require being recorded at two DSSs for daily periods lasting from 20 minutes to three hours, thus resulting in approximately 2×20^{10} bits of occultation data (with 8-bit analog-to-digital (A/D) conversion) per day. Further contributing to the large volume of data generated would be the large number of daily occultations--almost 100--which constituted the prime Pioneer Venus Orbiter Mission. This large volume of expected data strongly motivated the development of new conceptual designs for occultation data generation which would reduce the volume of raw occultation data while not compromising the scientific content of the data. In this context, the idea was conceived of using the predicted doppler frequency profile during atmospheric occultation to program the local oscillator in the open-loop receiver. As schematically illustrated in Figure 8, the mixed frequency product between the actual (acquired) signal frequency (f_a) and the predicted signal frequency (f_p) used to program the open-loop receiver local oscillator, becomes the "new" baseband frequency (f_a-f_p). This far less dynamic baseband frequency can now be passed through a correspondingly narrow filter and subsequently passed to the occultation data handling equipment. To recover the actual signal frequency (f_a), the experimenter simply combines the recorded signal frequency (f_a-f_p) and the local oscillator frequency (f_p). Based on the accuracy of the predicted doppler frequency profile, approximately 1 to 10 kHz at

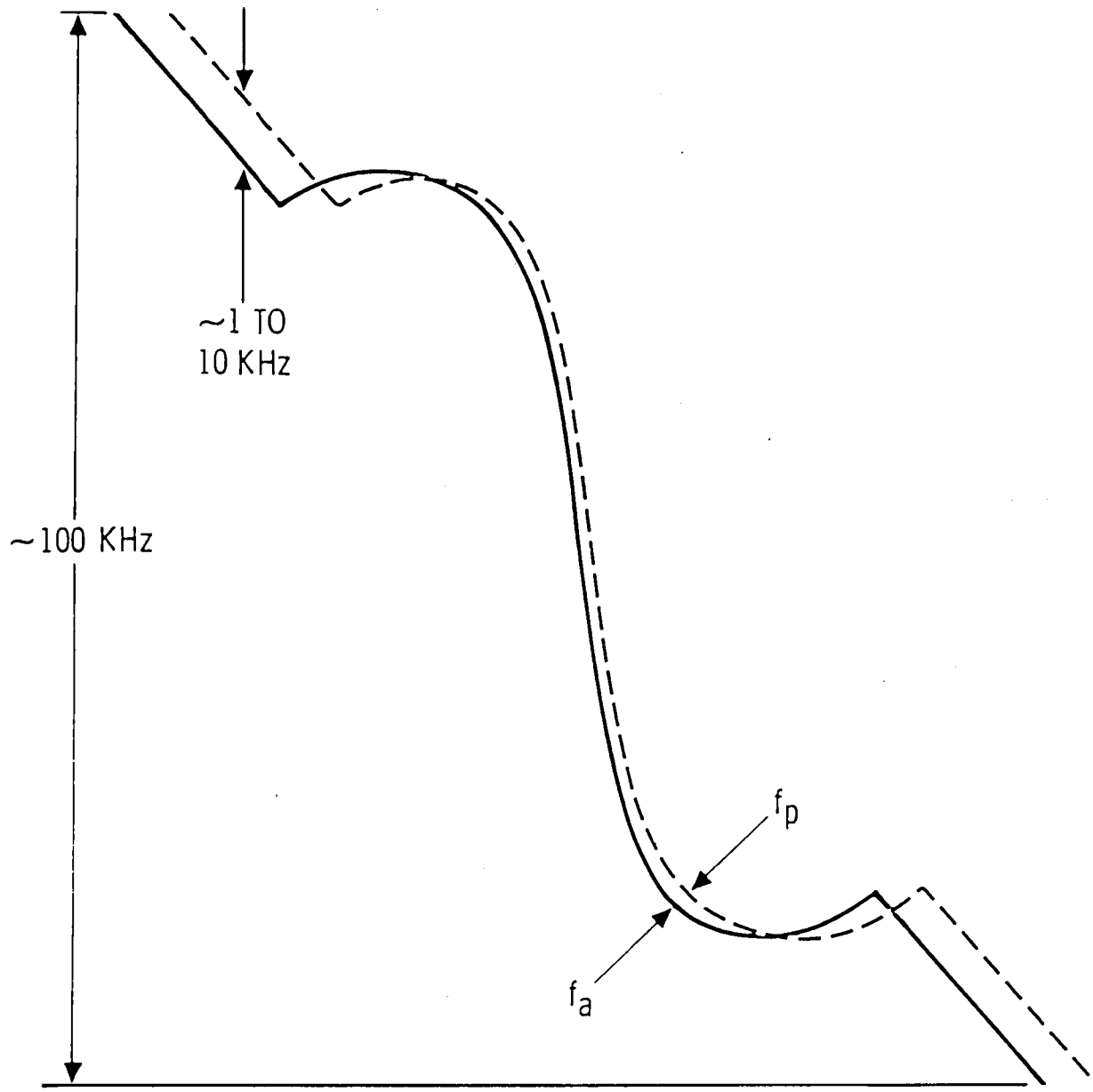

Figure 8. Actual and Predicted Signal Profiles

S-band, one could expect to reduce the required baseband frequency bandwidth, and hence the recorded data, by a factor of between 10 and 100. At such substantially reduced rates, one could also expect to be able to digitize and record the data on computer compatible magnetic tape in real time at the DSS, thus eliminating another costly step from the existing occultation system. Such a new capability, referred to as "real-time bandwidth reduction," was approved for implementation as one of the first operational capabilities of a new DSN Data System--The DSN Radio Science System. System design was initiated in 1976, and the operational capability was delivered in November of 1978.

The real-time bandwidth reduction system is briefly described in overview via a block diagram (Figure 9). Doppler frequency predictions which contain the effects of planetary atmospheric refraction are generated by software programs at JPL and subsequently transmitted to the DSS via high-speed data line (at 7.2 kbit/s). These predicts are formatted by the DSS occultation data handling equipment (Occultation Data Assembly or ODA) and are provided to a digitally controlled oscillator in the open-loop receiver. The resulting (bandwidth-reduced) baseband open-loop receiver output signal is provided to the ODA where it is digitized and written directly on computer compatible magnetic tape. This tape can either be shipped or replayed via high-speed data line (HSDL) to the Data Records Subsystem, where it is once again reformatted (Intermediate Data Record) and subsequently provided to the radio science experimenter.

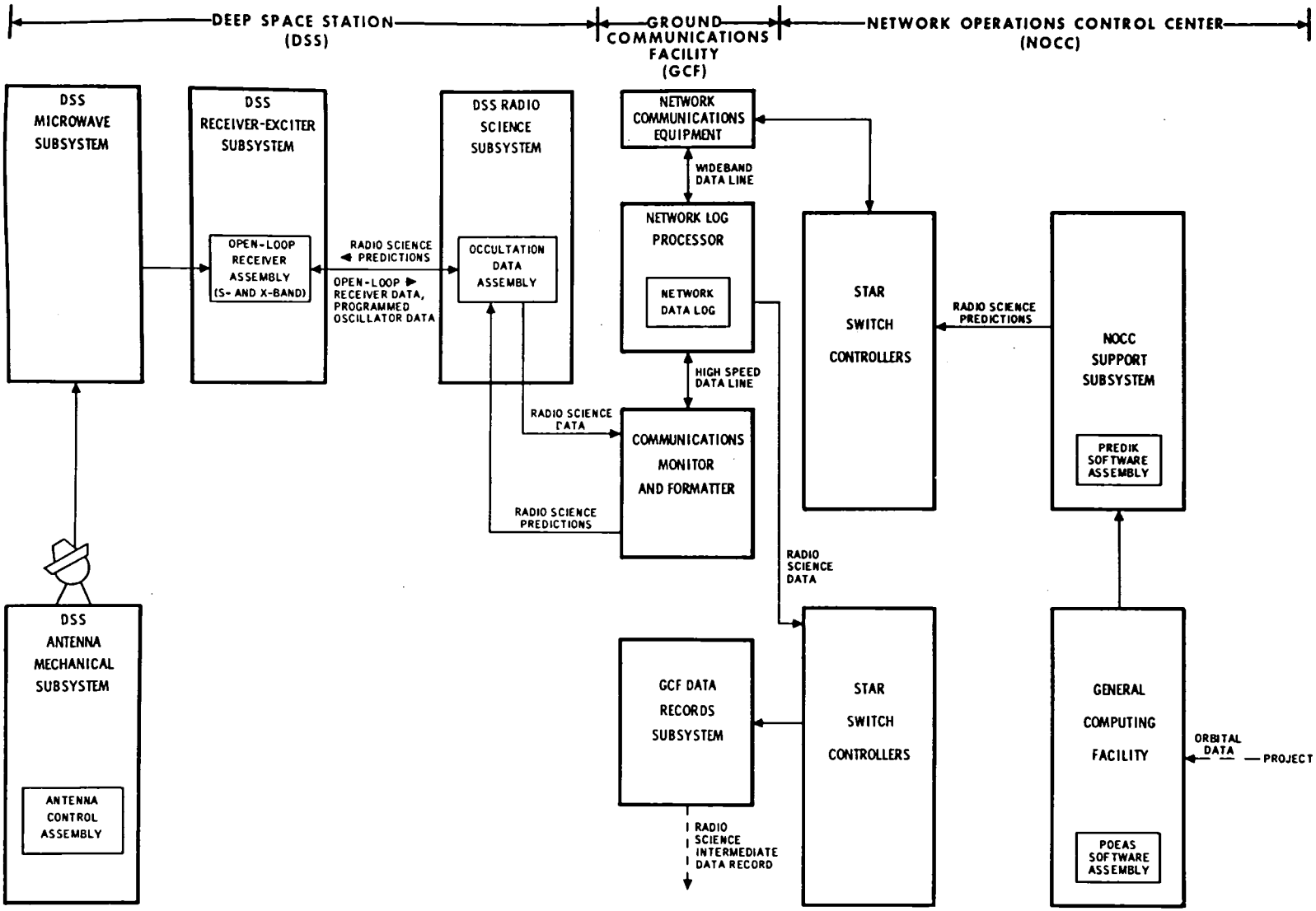

Figure 9. Real-Time Bandwidth Reduction Overview Block Diagram

A. REAL-TIME BANDWIDTH REDUCTION DETAILED DESCRIPTION

The real-time bandwidth reduction process begins with the production of the predicted doppler frequency profile which has been corrected for planetary atmospheric refractive bending. From this profile, a set of time-tagged (predicted) doppler frequencies is constructed. The number of points in any given set is controlled by experimenter input, which specifies the maximum allowable deviation from the instantaneous doppler profile of the linear interpolation between adjacent doppler frequency points. The set of doppler frequency points is transmitted via HSDL to the ODA. The ODA consists of a Modcomp II/25 Computer, Occultation Converter Subassembly (A/D and D/A converters), and Frequency Monitor Subassembly (doppler counter). The ODA computer converts the received doppler frequency points into an initial frequency and subsequent frequency rates (obtained by differencing adjacent frequency points and dividing by the time difference), and passes these to a digitally controlled oscillator in the Receiver-Exciter Subsystem. The digitally controlled oscillator is programmed by the ODA with an initial frequency and a series of frequency rates, which provide a piecewise linear frequency approximation of the dynamic occultation signal. At the highest expected frequency rates, the digitally controlled oscillator frequency error is less than 0.05 Hz--this error principally resulting from an approximate 30 microsecond delay in ramp initiation time. The digitally controlled oscillator frequency, slightly above 40 MHz, is multiplied up to S- and X-band to provide the first local oscillator frequencies. These are mixed with incoming spacecraft S- and X-band signals as provided at the output of the low-noise Traveling Wave Masers.

Depending on the estimated accuracy of the doppler frequency predictions, baseband filters in the receiver are selected from the available sets listed in Table I.

After filtering, the baseband signals are provided by the open-loop receiver to the Occultation Converter where they are sampled at the Nyquist rate and digitized with either 8 or 12 bit quantization, as selected by the experimenter. The standard Pioneer Venus Orbiter configuration of the ODA is two channels to accommodate the simultaneous transmission of S- and X-band signals. However, other ODA configurations, in terms of number of channels, and maximum baseband bandwidth per channel, are available and are listed in Table II.

Subsequent to digitization, the ODA computer time-tags and writes the data on magnetic tape (Original Data Record or ODR). ODA timing is controlled by frequency and timing pulses from the FTS. The FTS utilizes either Cesium or Hydrogen Masers as the prime frequency reference, achieving frequency stabilities on the order of 10^{-13} or better.

As the ODR is being written, the ODA passes the digitized signal back through a D/A converter, and then passes this reconstructed analog signal back to a real-time spectrum analyzer for real-time validation of the data generation process at the DSS. Finally, the digitally controlled oscillator frequency (slightly above 40 MHz) is down-converted to a few MHz to obtain better counting resolution, counted by a frequency counter to an accuracy level of 0.5 Hz S-band, and written by the ODA computer on the same magnetic tape as are the occultation signals. The digitally controlled oscillator programmed frequencies are also recorded. Subsequent to data generation, a

TABLE I

Available S- and X-Band Filter Pairs

S-Band	X-Band
1.0 kHz	3.0 kHz
2.5 kHz	7.5 kHz
5.0 kHz	15.0 kHz
10.0 kHz	30.0 kHz

TABLE II

Available Channel Configurations of the ODA

Frequency Channels	Maximum Baseband Bandwidth/Channel
1	40 kHz
2	20 kHz
2	10/30 kHz (standard configuration
4	10 kHz

portion of the ODR (which contains both the occultation data and digitally controlled oscillator frequency history) can be replayed via HSDL for a quick-look analysis, or the entire ODR can be replayed for processing into the final experimenter data record. Alternately, the ODR can be shipped back to JPL and converted directly into an experimenter data record by the experimenter.

The real-time bandwidth reduction process described in this section is schematically illustrated in Figure 10.

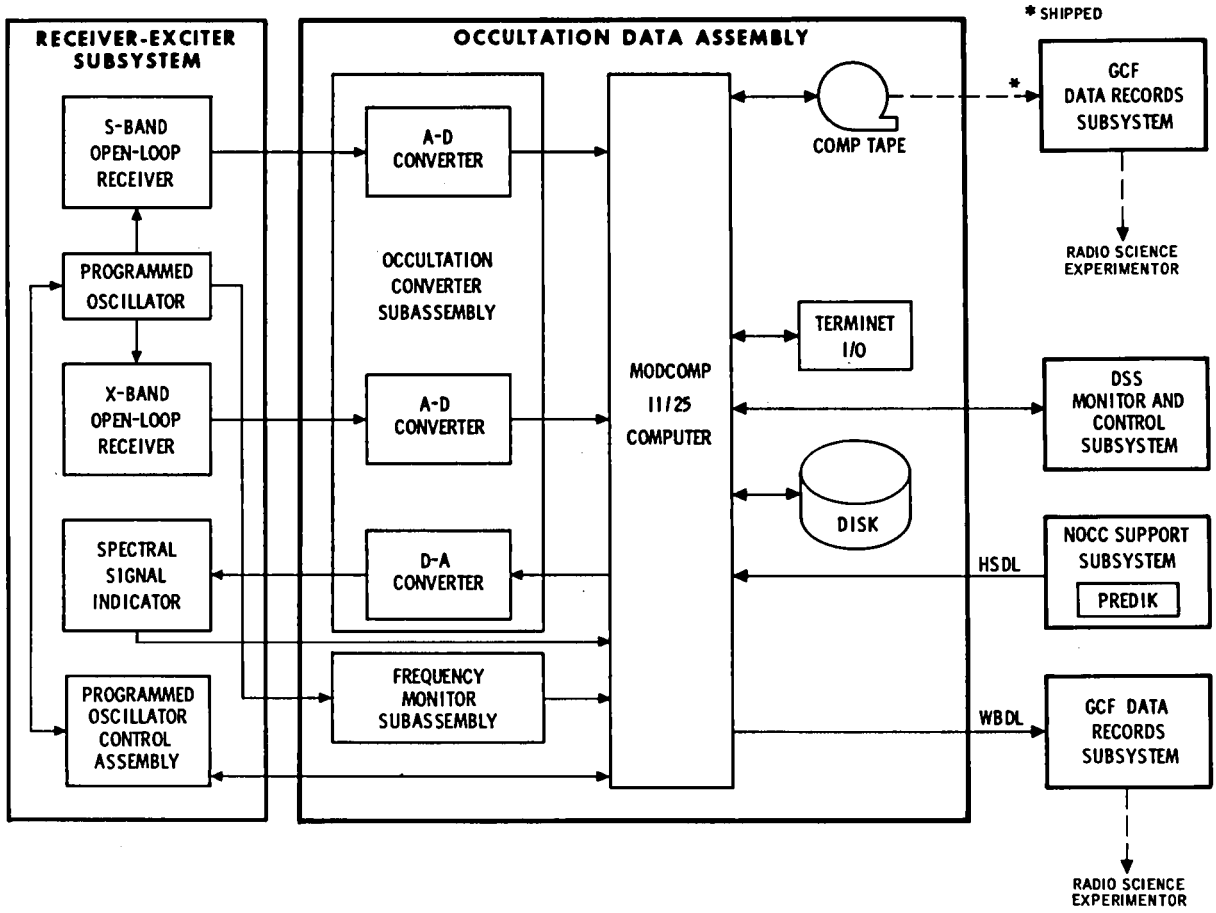

Figure 10. Occultation Data Assembly Block Diagram

B. PRELIMINARY RESULTS OF PIONEER VENUS USAGE OF REAL-TIME BANDWIDTH REDUCTION DURING THE PIONEER VENUS MISSION

Although confirming statistics are not readily available, the analog occultation data generation system in use prior to the Pioneer Venus Mission was generally considered to yield only 50% good (i.e., useable) data. It is felt that this low rate of data return resulted principally from (1) lack of operator familiarity, and (2) the R & D or prototype, rather than operational, status of the equipment.

The real-time bandwidth reduction system was first used operationally during the Pioneer Venus Orbiter prime mission. Between December 1978 and May 1979 the system was in operation variously at DSS 14 (Goldstone, California), DSS 43 (Canberra, Australia), and DSS 63 (Madrid, Spain). Overall occultation data recovery during this period is estimated at 82%, after losses caused by all sources, including (1) DSS hardware, (2) DSS software, (3) doppler frequency prediction software, and (4) operational errors. In addition, since each DSS had a wide bandwidth backup occultation system at S-band (i.e. fixed frequency first local oscillator in the open-loop receiver), all S-band data was essentially recovered, thus reducing the total of data irretrievably lost to about 10%. Considering that this was the first usage of a multifacility, large-scale hardware, software, and operator system, the data recovery figure of 82% is viewed favorably.

VIII. MEDIUM BANDWIDTH
RADIO SCIENCE SYSTEM CAPABILITY--THE SATURN RING EXPERIMENT

Medium bandwidth radio science system capability was implemented in response to requirements imposed by the Saturn Ring Experiment, performed on November 13, 1980, as Voyager 1 flew by Saturn. The goals of this experiment were described by Eshleman et al. (1977):

> "The goals of these observations are to measure the complex (amplitude and phase) radio extinction and angular scattering function of the rings as a function of wavelength, polarization, and radial distance from Saturn. These observations would then be used to infer the first several moments of the ring particle size distribution, the total amount of material in the rings, the radial distribution of that material, and limits to possible particle shapes and constituents."

To perform the experiment, the ring scattered Voyager 1 S- and X-band signals were required to be recorded in both right and left circular polarization (RCP-LCP) modes. To record a sufficient baseband signal output which would accommodate both trajectory prediction uncertainties and the major portion of the (scattered) signal power, bandwidths were required as follows:

(1) S-band: 50 kHz
(2) X-band: 150 kHz

Radio frequency phase stability requirements were quite stringent. The maximum deviation after calibration from an ideal linear phase response (1000 second averaging period) was:

(1) Single S-band channel: 36 deg
(2) Single X-band channel: 132 deg
(3) Differenced S-X channel (S-band - (3/11) X-band): 10 deg
(4) Differenced RCP and LCP channels (both S- and X-band): 1 deg

The medium bandwidth radio science capability implemented in response to the Voyager Saturn Ring Experiment requirements is described below by subsystem function.

A. THE NOCC RADIO SCIENCE SUBSYSTEM

The Network Operations Control Center (NOCC) Radio Science Subsystem (NRS) provided two main functions during the Saturn Ring Experiment: radio science frequency predictions and real-time system performance validation.

Radio science frequency predictions are generated by the "POEAS" software program following receipt of a spacecraft state vector from the flight project. The POEAS program generates frequency-independent observables which have been corrected for planetary atmospheric refraction. These data are written on magnetic tape and are passed to the NOCC Support Subsystem.

In performing real-time system performance validation, digital data originating from the DSS Spectral Signal Indicator (SSI) are reconstructed into spectral displays and are provided on digital television in the NOCC and the project radio science area via the Display Subsystem.

B. THE NOCC SUPPORT SUBSYSTEM

The NOCC Support Subsystem utilizes the software program "PREDIK" to generate frequency-dependent radio science predictions for the Deep Space Stations. Inputs are POEAS output from the NRS and spacecraft frequencies from the flight project. The output is radio science frequency predictions which are transmitted via HSDL to the DSS Radio Science Subsystem.

C. THE ANTENNA MICROWAVE SUBSYSTEM

The Antenna Microwave Subsystem (UWV) provides S-and X-band signals that are both right circularly polarized and left circularly polarized via an orthomode polarizer. The Antenna Microwave Subsystem functional block diagram is seen in Fig. 11.

D. THE RECEIVER-EXCITER SUBSYSTEM

The Receiver-Exciter Subsystem (RCV) provided two main functions during the Saturn Ring Experiment: acquisition of four signals simultaneously and real-time spectral analysis of a reconstructed analog signal received from the DRS.

The RCV utilizes the four-channel medium bandwidth Multimission Open-Loop Receiver (MMR) to acquire the four signals (permutations of S- and X-band, and LCP and RCP) simultaneously. The MMR contains a programmed oscillator that heterodynes the signals down from S- and X-band to medium bandwidth. The programmed oscillator is driven by a (predicted) frequency profile provided by the ODA. The output medium bandwidth signals are appropriately filtered and provided to the Medium Bandwidth Converter Subassembly. Amplitude response requirements on the output bandwidth are:

(1) The usable bandwidth, defined by the -1 dB points, is > 83% of the output bandwidth

(2) $\pm$37% of the output bandwidth relative to the bandpass center has an amplitude ripple < $\pm$0.2 dB

(3) The "rejection" bandwidth, defined by the -23 dB points, is < 117% of the output bandwidth

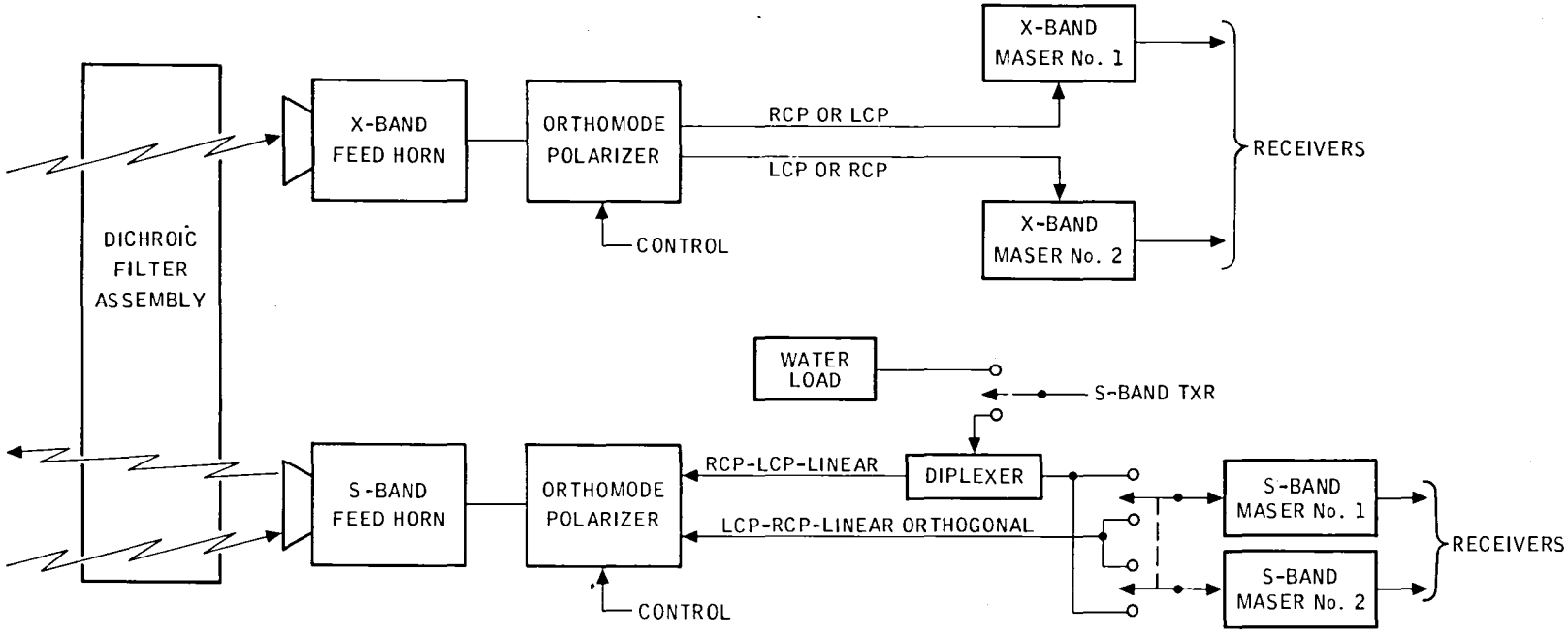

Figure 11. Antenna Microwave Subsystem Functional Block Diagram

The programmed oscillator frequency (initially at 41 MHz) is heterodyned down to the MHz level and provided to the Radio Science Subsystem for recording. A functional block diagram of the Multimission open-loop receiver is seen in Fig. 12.

During MMR operations, the RCV is supplied with a reconstructed medium bandwidth signal by the ODA. This signal is analyzed by the Spectral Signal Indicator (SSI), which generates and outputs real-time spectrum displays. These displays are provided to the ODA in digital form for eventual remote display in the NOCC.

E. THE RADIO SCIENCE SUBSYSTEM

The Radio Science Subsystem (DRS) performs the major functions of providing the predicted doppler profile to the programmed oscillator and the subsequent digitization and recording of the receiver medium bandwidth output signals.

Radio science predictions in the form of frequency and time pairs are received by the ODA. These are converted to an initial frequency and subsequent frequency rates and provided to the Programmed Oscillator Control Assembly.

The four signals output by the MMR are digitized with 8 bit quantization by the Medium Bandwidth Converter and recorded on the Digital Recording Assembly (DRA). Recorded data is time tagged with the following accuracies:

1. Time tag offset from station time: 10 microseconds
2. Sampling rate accuracy: $10^{-5} \cdot (\text{bandwidth})^{-1}$
3. Sampling jitter: $(2^{8} \cdot \text{bandwidth})^{-1}$

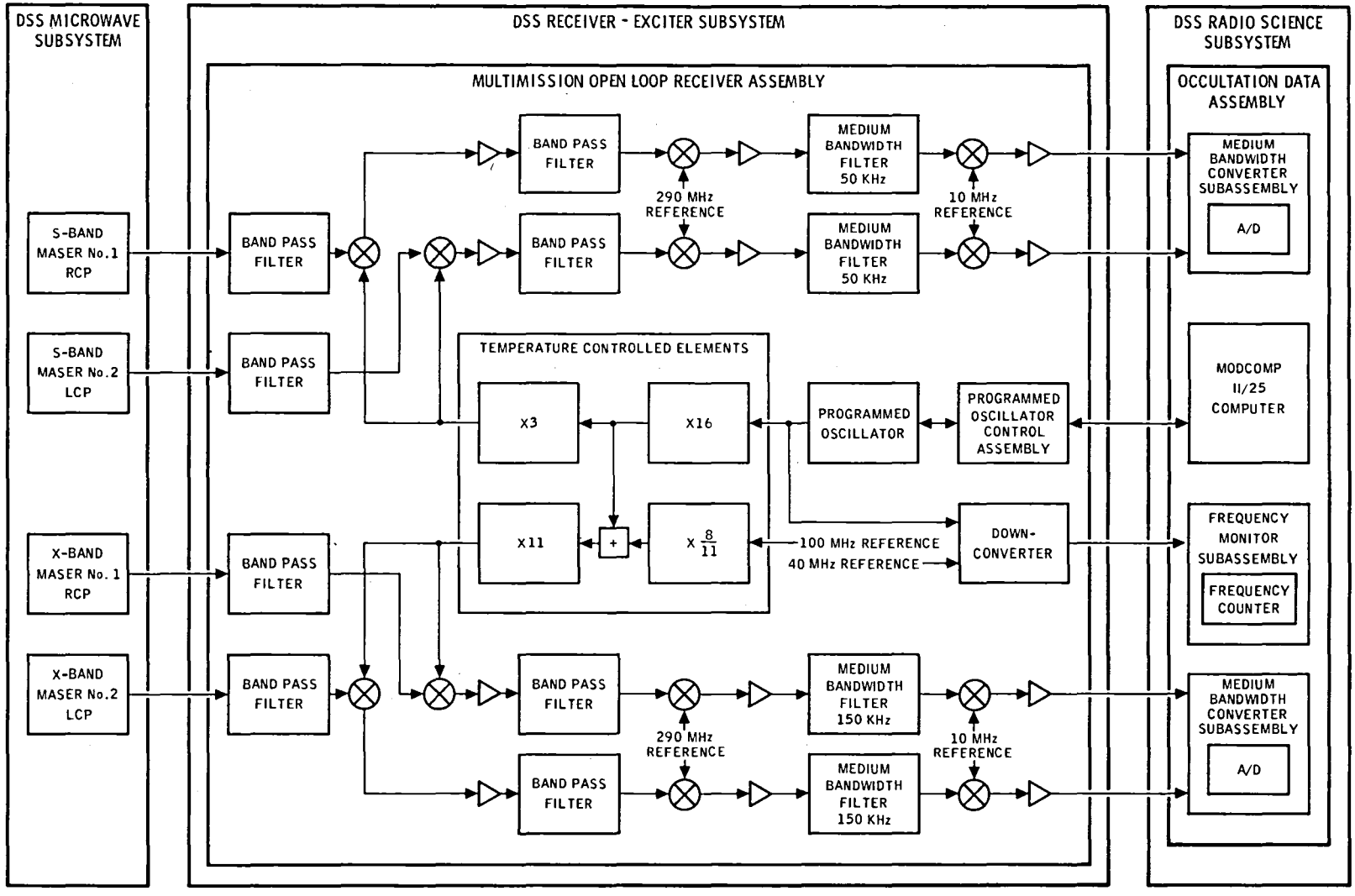

Figure 12. Multimission Open-Loop Receiver Functional Block Diagram

The MMR provides the down-converted programmed oscillator frequency to the Frequency Monitor, where it is counted and recorded at one second intervals on the integer second by the ODA. The accuracy of the recorded frequency is < 0.5 Hz at S-band (rms). The ODA also records the frequency predictions provided to the programmed oscillator, as well as the commanded programmed oscillator frequencies on integer second intervals.

A reconstructed analog signal is provided to the SSI, and the resulting digital spectrum data from the SSI are received by the ODA, formatted for, and transmitted via wideband data line to the NOCC.

The ODA provides real-time status, configuration, and alarm data locally at the DSS and via HSDL to the NOCC.

Subsequent to the generation of radio science data, the ODA and DRA recorded tapes are shipped to the Network Radio Science Subsystem for further processing. A functional block diagram of the Radio Science Subsystem is provided in Fig. 13, while Fig. 14 provides a Digital Recording Assembly functional block diagram.

F. THE NETWORK RADIO SCIENCE SUBSYSTEM

The Network Radio Science Subsystem receives the DRA recorded data from the DSS, plays back the DRA recorded data and rewrites (one signal per pass through) the digitized data on computer-compatible tapes. These tapes plus the ODA recorded tapes, which contain the programmed oscillator information, constituting the sum total of radio science data, are then delivered to the flight project.

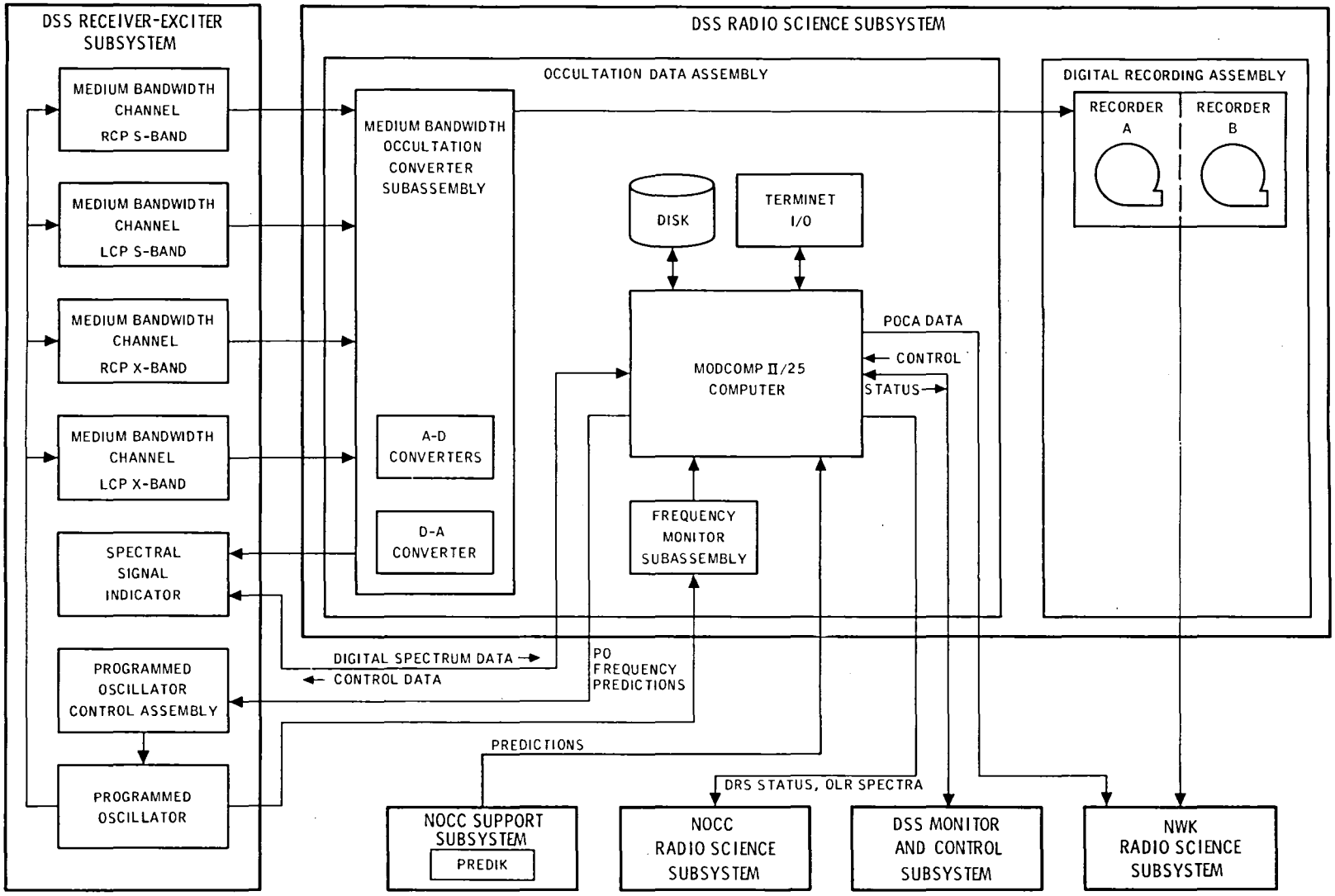

Figure 13. Radio Science Subsystem Functional Block Diagram

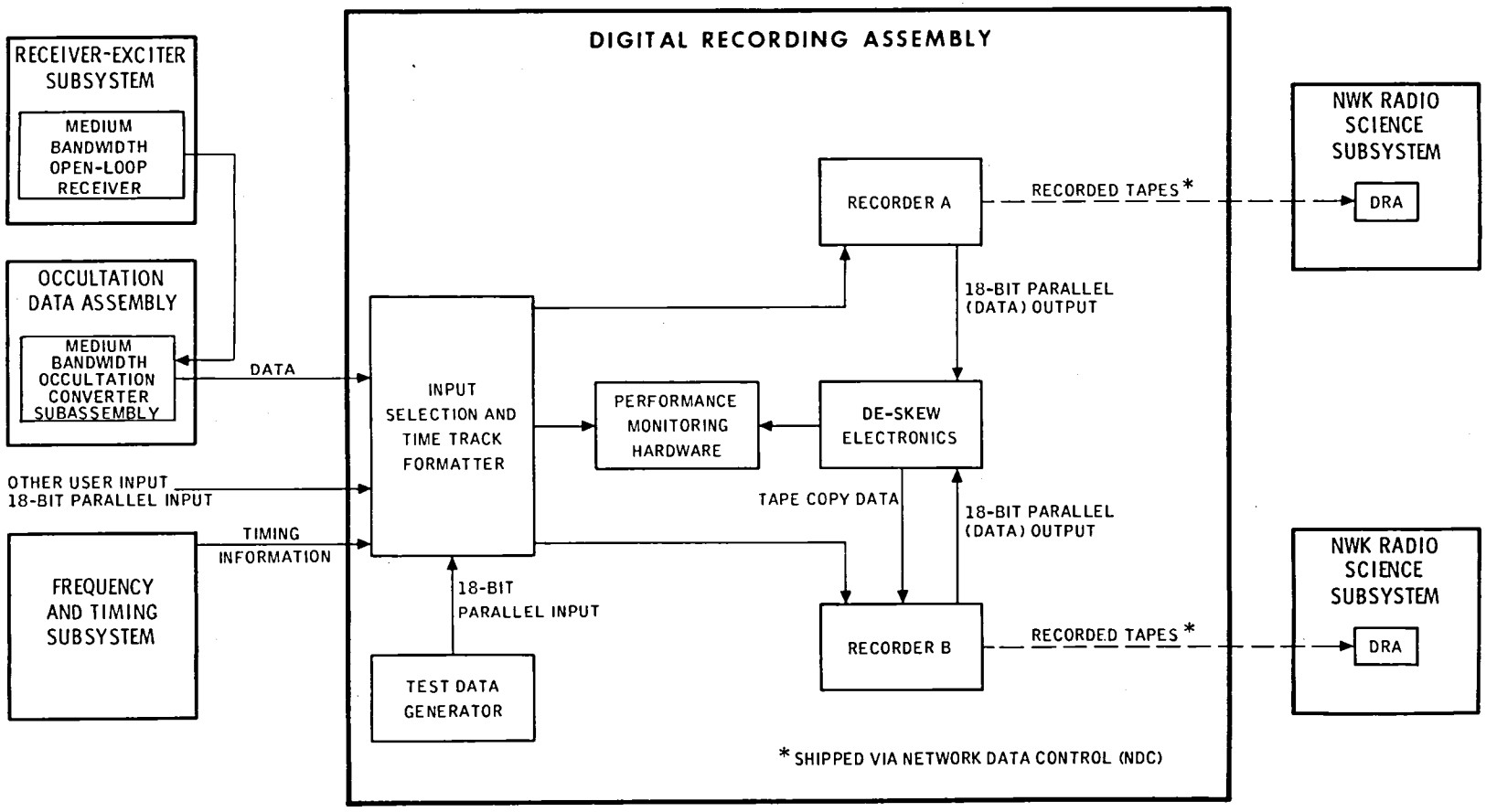

Figure 14. Digital Recording Assembly Functional Block Diagram

IX. MONITOR AND CONTROL OF RADIO SCIENCE OPERATIONS

Extensive capabilities have been installed at both the Deep Space Stations and the Network Operations Control Center (NOCC) at JPL for monitoring and control of critical radio science events. Adhering to the DSN philosophy of centralized control at JPL and automation at the DSS, equipment status and quick-look radio science data are brought back to NOCC for real-time analysis by joint teams composed of radio science experimenters and DSN radio science system engineers. This team also initiates required configurational changes in the radio science equipment at the DSS during critical radio science events.

Monitor and validation of radio science data is accomplished via three major NOCC Radio Science Subsystem (NRS) capabilities:

(1) Graphical display of radio metric data
(2) Graphical display of open-loop spectral data
(3) Alphanumeric displays of radio science equipment status and configuration

These are described in detail below.

A. GRAPHICAL DISPLAY OF RADIO METRIC DATA

Various radio metric data are accumulated, processed, and formatted in the Metric Data Assembly of the Tracking Subsystem. These data are then provided to the Communications Monitor and Formatter for subsequent HSDL transmission to the NOCC Tracking Subsystem. After additional processing by the NOCC Tracking Subsystem, the radio metric data are provided to the NRS. The data are processed into graphical displays and are provided to the Display Subsystem for display in the NOCC and the project radio science areas. Up to 12 separate parameters can be displayed simultaneously, and hard copies can be

made. Operators construct and control the graphical displays through operator control instructions (OCI) that are entered into the Display Subsystem.

B. GRAPHICAL DISPLAY OF OPEN-LOOP SPECTRAL DATA

Digital spectral data from the SSI are transferred to the ODA. The ODA formats and transmits the data to the NRS via wideband data line. The NRS reconstructs the open-loop spectra and provides such replicated spectra to the Display Subsystem for display in the NOCC and project radio science areas. The spectral display is composed of 400 bins, and the (full scale) amplitude is selectable from the following:

(1) 18.75 dB
(2) 37.5 dB
(3) 75 dB
(4) 150 dB

The display is updated every five seconds. In addition, the display identifies the frequency and amplitude of the maximum power point. NOCC operators control the open-loop spectra displays through OCI inputs to the Display Subsystem.

C. ALPHANUMERIC DISPLAY OF RADIO SCIENCE EQUIPMENT STATUS AND CONFIGURATION

DSS Radio Science Subsystem status, configuraton, and control data during radio science operations are formatted by the ODA and passed to the Communications Monitor and Formatter for subsequent HSDL transmission to the NRS. The NRS formats this data into displays and provides the data to the Display Subsystem for display in the NOCC. Status displays include:

(1) Program mode (idle, run, playback, etc.)

(2) Hardware status, including:

(a) Frequency Monitor

(b) Modcomp Computer

(c) Magnetic tape units

(d) Programmed Oscillator Control

(e) Occultation Converter

Configuration displays include:

(1) Receiver channel select

(2) A-D conversion mode

(3) Sampling rates

(4) SSI channel select

(5) Receiver filter select

while control data displays include:

(1) Predicts set ID

(2) Frequency Monitor frequency

(3) Frequency offsets

(4) Time offsets

(5) Time-tagged Programmed Oscillator frequency

(6) Time-tagged Programmed Oscillator frequency rate

NOCC operators control the DRS status, configuration, and control data displays through OCI inputs to the Display Subsystem.

Figure 15 illustrates the NOCC Radio Science Subsystem functional block diagram, while Figure 16 presents a sample open-loop spectral display.

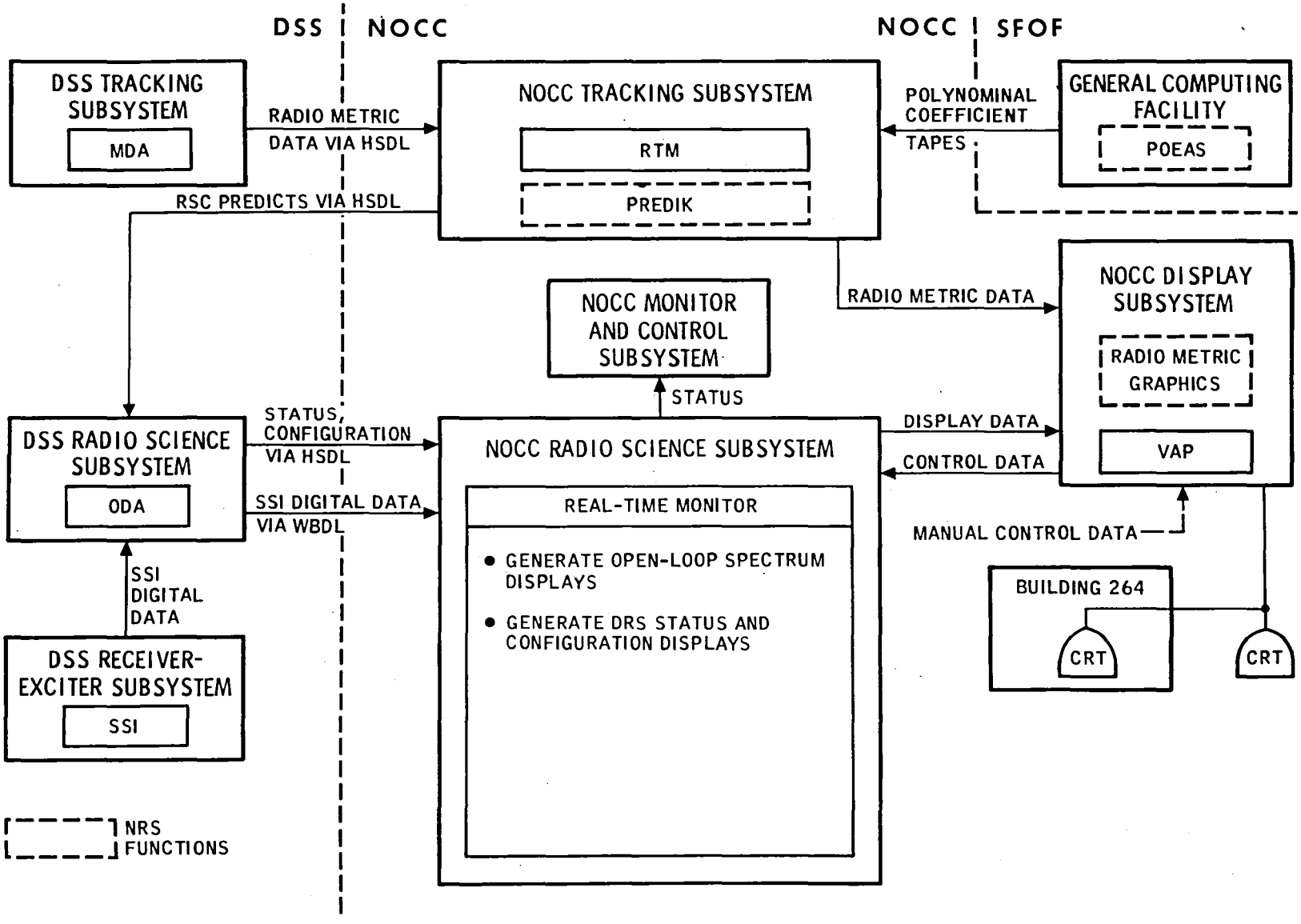

Figure 15. NOCC Radio Science Subsystem Functional Block Diagram

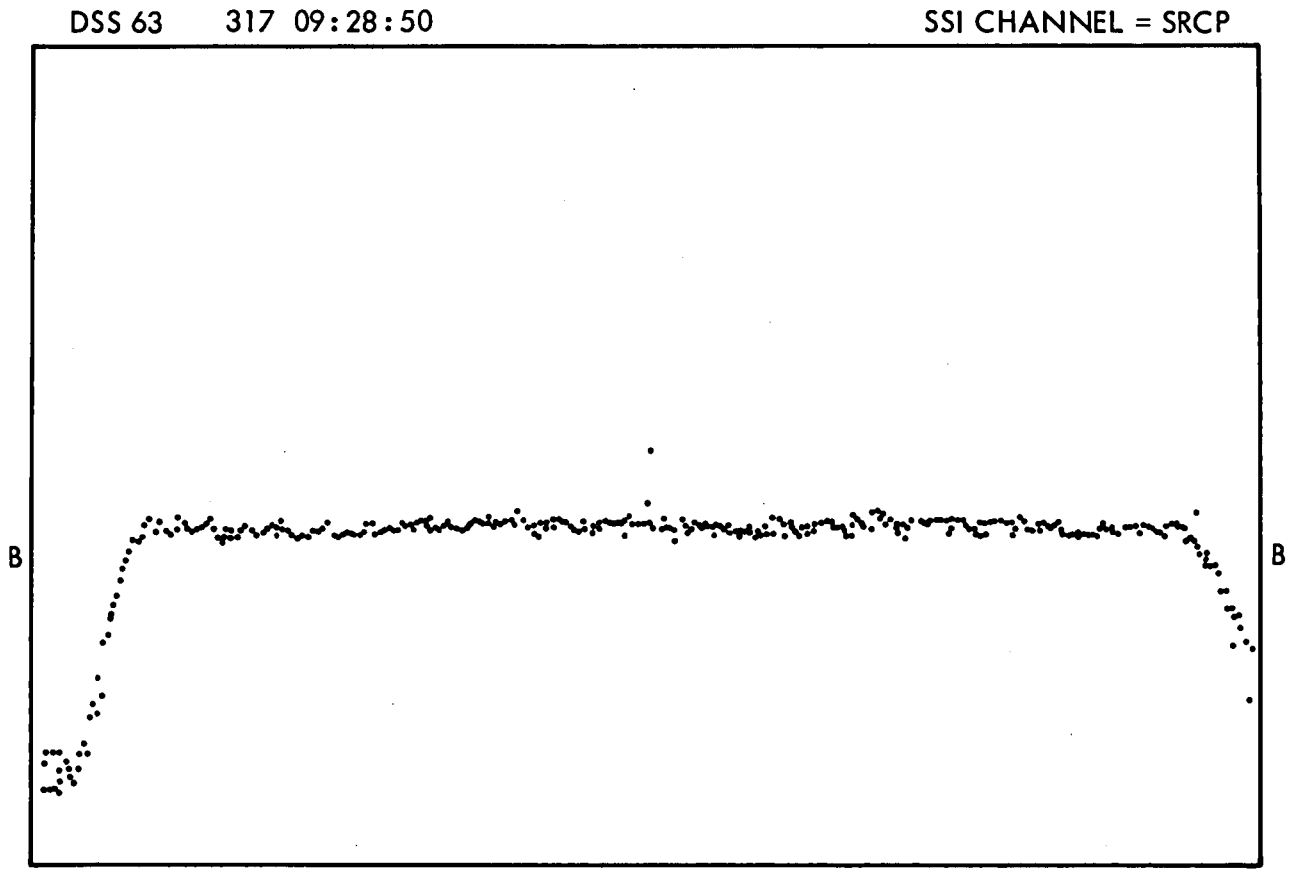

FULL SCALE AMPLITUDE = 150.0 DB
FULL SCALE BANDWIDTH = 50 K Hz
AVERAGE NUMBER SPECTRA = 128
TRANSFORM SIZE = 1024
MAX PWR POINT = RSNR 19 AT FREQ OF 25 K Hz

Figure 16. Open-Loop Spectral Display

X. THE GALILEO FARADAY ROTATION EXPERIMENT

The Galileo Radio Science Team has proposed an experiment to ascertain magentic field characteristics in the Jovian ionosphere and plasmasphere and the solar corona phases of the Galileo mission through Faraday rotation measurements. The experiment requires a linearly or elliptically polarized downlink signal, coupled with the capability to obtain dual-frequency range measurements. Faraday rotation provides information on the product of the magnetic field and electron density, while the dual-frequency range measurements provide the integrated electron density, hence allowing solutions for the magnetic field strength and direction. Since the Galileo spacecraft is rotating, the fundamental experiment requirements become:

> "measure and record the polarization angle of a rotating linearly or elliptically polarized S-band signal"

The accuracy requirement for multiple polarization angle measurements during a five hour period is <2.3 deg rms. In addition, a real-time readout capability with a 1 deg resolution requirement is necessary for purposes of validation.

The equipment necessary to obtain and record the polarization data will for the most part consist of the existing open-loop radio science equipment. Figure 17 is a functional block diagram of the proposed system. The Galileo S-band signal is separated into LCP and RCP components in the orthomode polarizer, and after low-noise amplification, the two signal components are heterodyned down to baseband in dual channels of the multimission open-loop receiver. Within the Radio Science Subsystem, the signals are digitized and recorded via a Mod-Comp II minicomputer. Subsequently, the recorded signals are processed to retrieve the polarization angle versus time. A pilot tone is injected at the horn feed to provide phase calibration of the RCP and LCP channels, while the receiver outputs are provided to a real-time spectrum analyzer for real-time polarization angle readout.

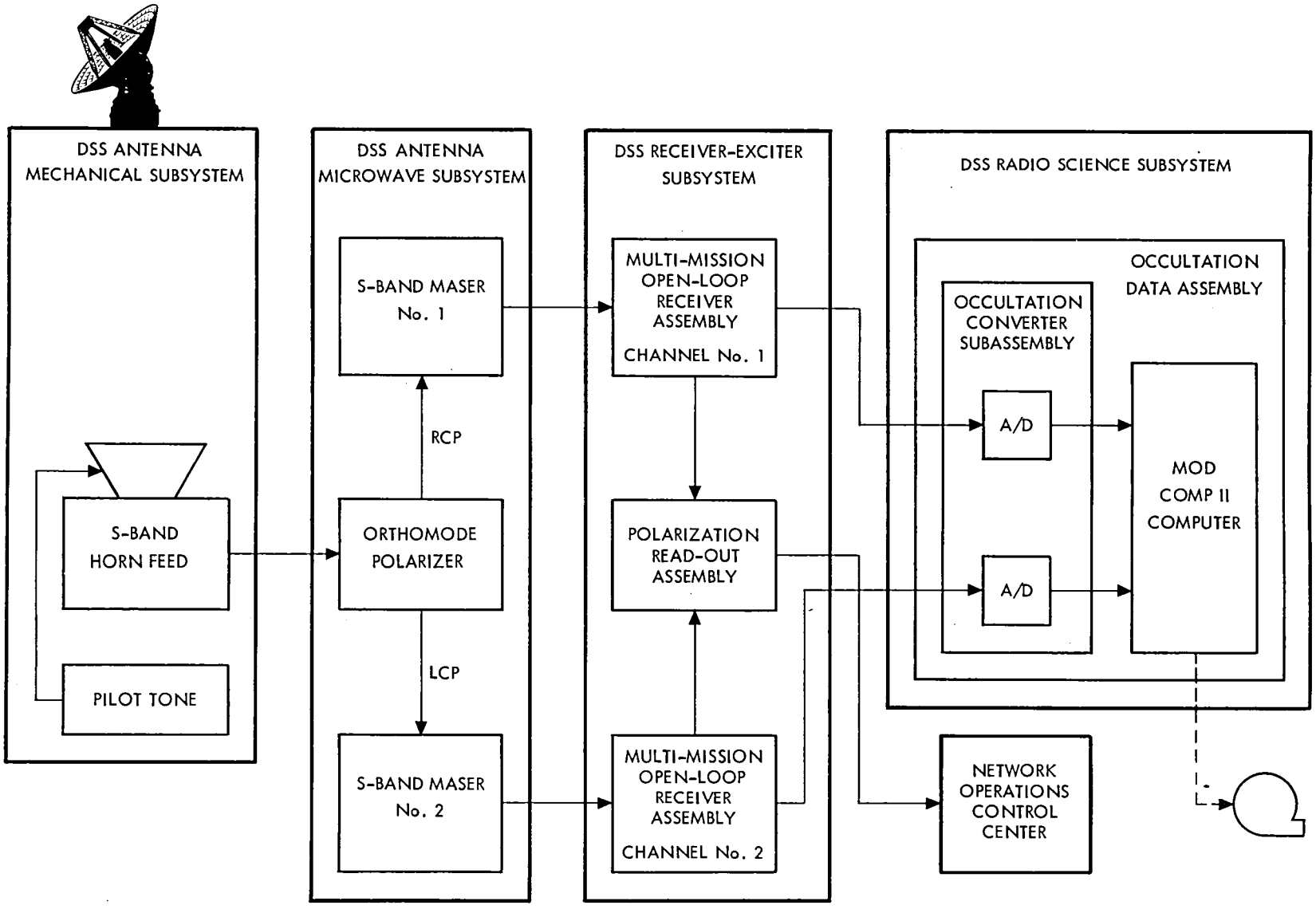

Figure 17. Galileo Faraday Rotation Experiment Functional Block Diagram

XI. GRAVITATIONAL PHYSICS: THE FUTURE CHALLENGE OF DSN RADIO SCIENCE

One of the most exciting challenges facing gravitational theoreticians and experimenters in the remaining decades of the 20th century will be the attempted detection and measurement of "gravitational waves" as predicted by Einstein's General Theory of Relativity. Gravitational waves are spatial strains propagating at the speed of light which are (expected to be) generated by the violent collapse of stars, star clusters, galaxy cores, quasars, and Seyfert galaxies into supermassive black holes (Thorne and Braginsky, 1976). Proposals have been advanced to use "ultraprecise" two-way doppler data while tracking spacecraft at large distances (i.e., 1 AU) to detect very-low-frequency ($\sim 10^{-3}$ Hz) gravitational waves (Davies, 1974; Estabrook and Wahlquist, 1975). Although such a detection scheme appears to be one of the more promising techniques suggested, substantial improvements in current Deep Space Network and spacecraft performance will have to be achieved, as well as provision of new capabilities, to bring to fruition the utilization of ultraprecise doppler data in the search for gravitational waves.

As already noted, gravitational waves are (expected to be) produced by the violent collapse of stellar bodies into supermassive black holes; these waves are expected to be evidenced as spatial strains propagating at the speed of light. Specifically, one expects that the waves will:

(1) Alter the distance between separated free masses.

(2) Produce a fractional frequency shift in ultraprecise doppler data, on the order of the wave amplitude.

Thorne and Braginsky have estimated possible gravitational wave characteristics; these are presented in Fig 18. As can be seen, the wave

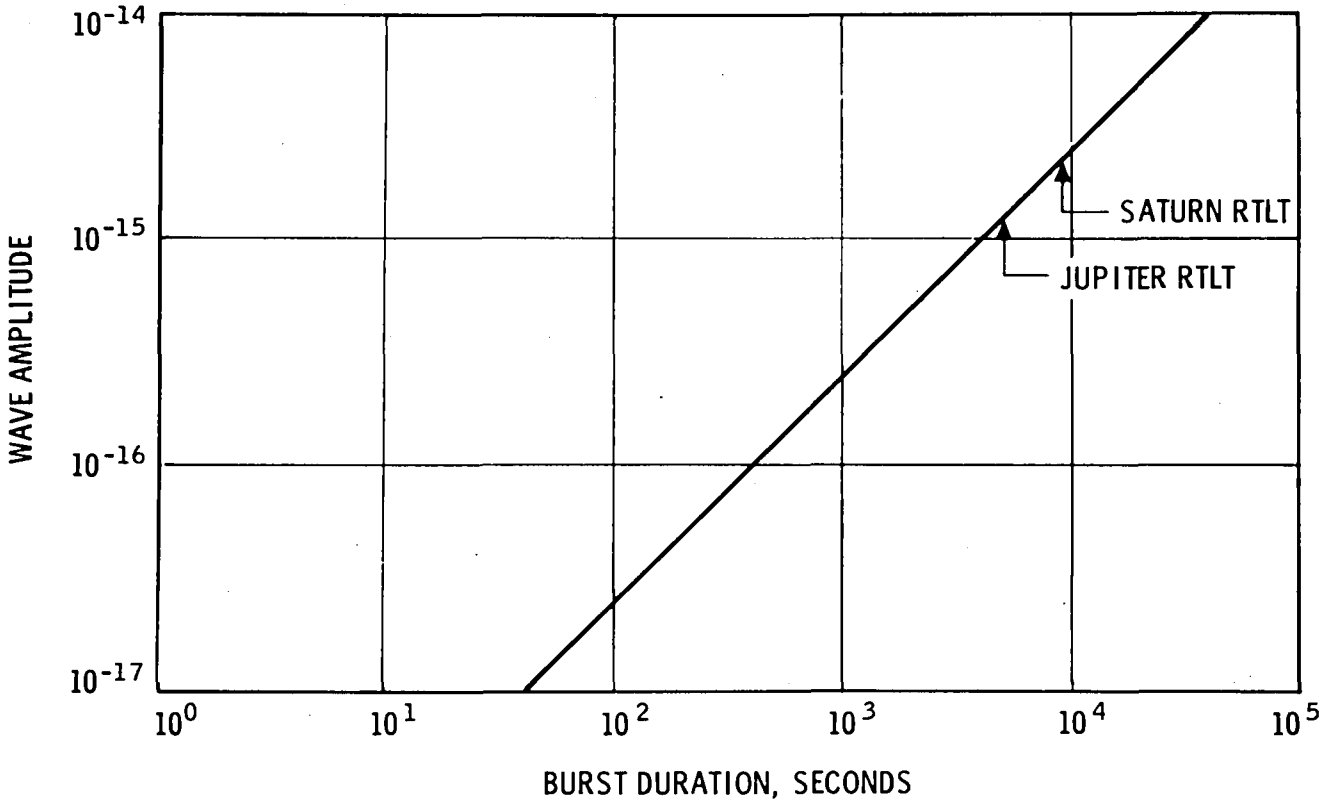

Figure 18. Relationship Between Gravitational Wave Amplitude and Burst Duration

duration (τ_a) is proportional to the wave amplitude (h) and the expected ranges of durations and amplitudes are:

$$40 \text{ seconds} \leq \tau_a \leq 40{,}000 \text{ seconds}$$

$$10^{-17} \leq h \leq 10^{-14}$$

The special feature which allows the usage of ultraprecise doppler data for the possible detection of gravitational waves is a unique "three-pulse" signature which is a function of the spacecraft, Earth, and gravitational wave propagation direction geometry. The pulses (fractional frequency shifts) result from effects which are conveniently described as follows:

(1) "Clock speed-up" (Earth only effect)

(2) "Buffeting" (equal Earth and spacecraft effect)

Consider a case where θ defines the angle between the gravitational wave propagation direction and the Earth-spacecraft line, as seen in Fig. 19. Clock speed-up is evidenced as pulses of maximum amplitude -h and +h at the time the wave impinges on Earth and a round-trip-light-time (RTLT) later, respectively. This is shown schematically in Fig. 20. Similarly, Earth buffeting is seen as pulses of maximum amplitude $+h \cos\theta$ when the wave impinges on Earth and a RTLT later. In addition, spacecraft buffeting produces a pulse of $-2h \cos\theta$ in the doppler data a one-way-light-time after the wave strikes the spacecraft. Earth and spacecraft buffeting effects are schematically illustrated in Fig. 21. Finally, combining the clock speed-up and Earth and spacecraft buffeting effects, one obtains the unique three-pulse signature which is expected to be seen in ultraprecise two-way doppler data. The characteristics of this signature are as follows:

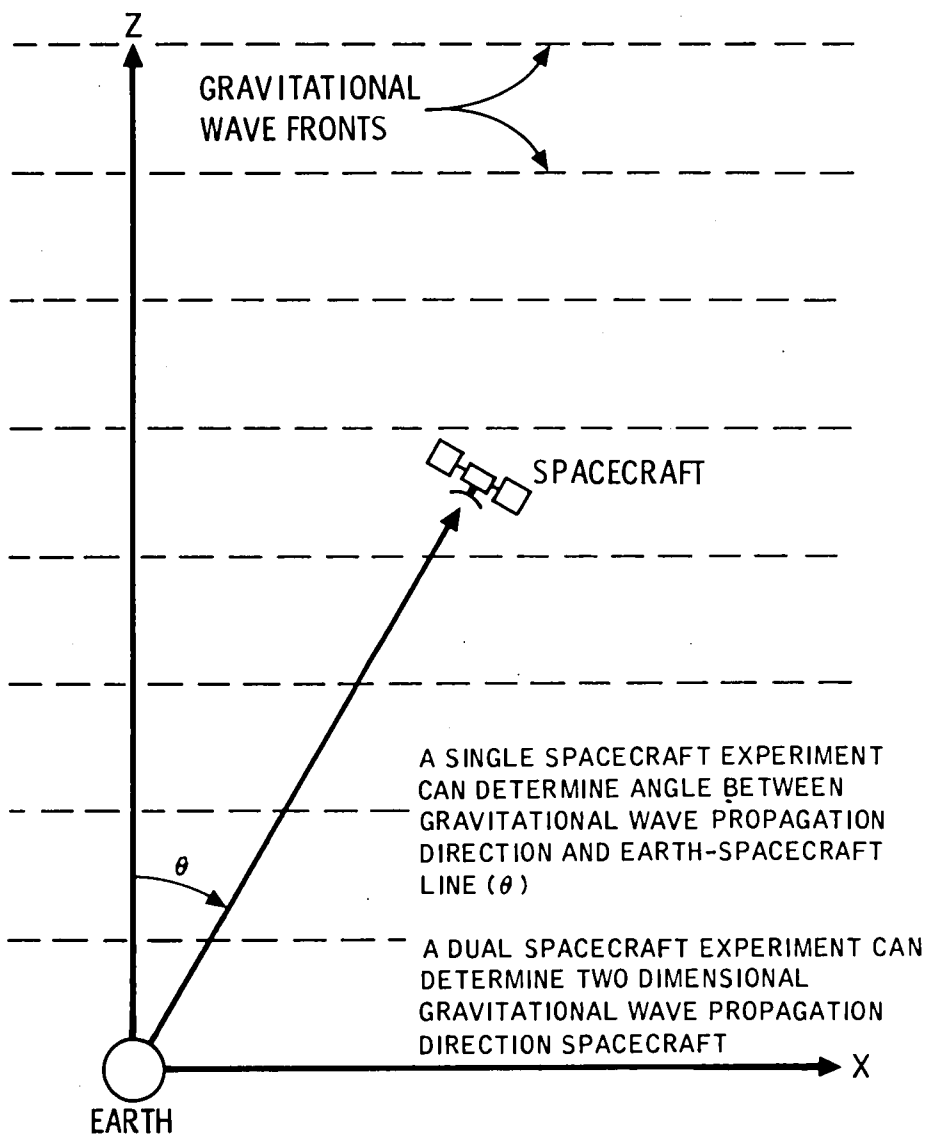

Figure 19. Gravitational Wave Geometry

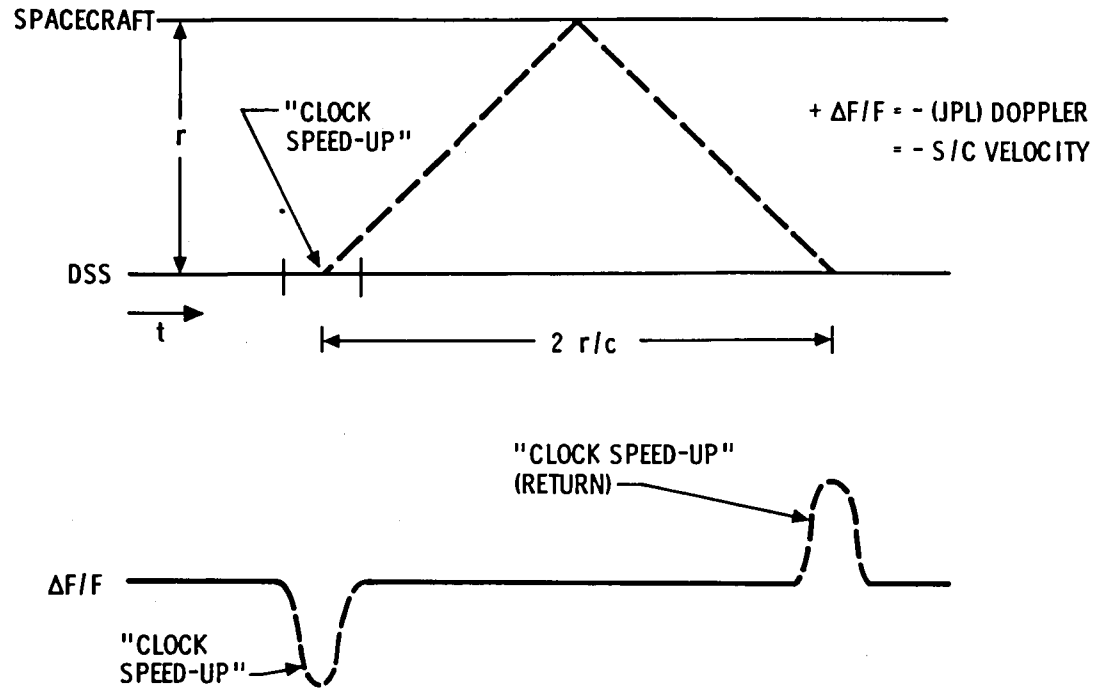

Figure 20. Clock Speed Up Signature in Ultraprecise Doppler Data

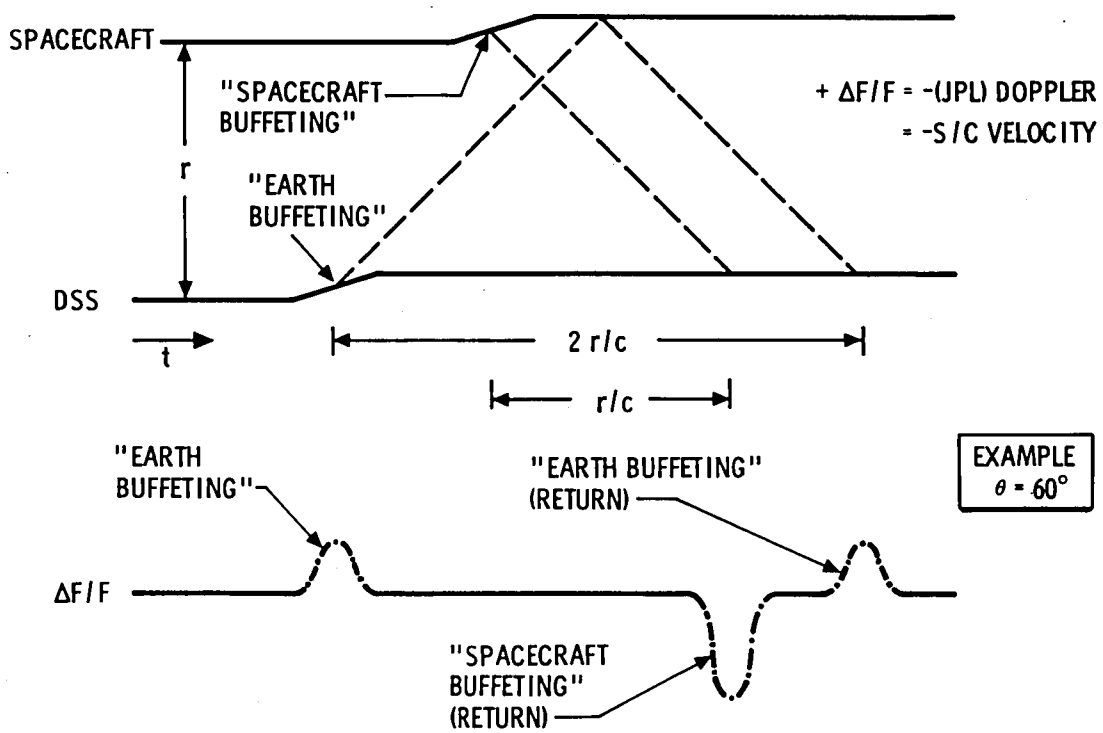

Figure 21. Earth and Spacecraft Buffeting in Ultraprecise Doppler Data

(1) Pulse amplitudes

(a) $h(\cos\theta - 1)$

(b) $h(-2\cos\theta)$

(c) $h(\cos\theta + 1)$

(2) Pulse separation times (r = Earth-spacecraft distance)

(a) $rc^{-1}(1 + \cos\theta)$

(b) $rc^{-1}(1 - \cos\theta)$

Figure 22 schematically demonstrates the combination of clock speed-up and buffeting effects for θ = 60 degrees.

From the above, it is easy to see that the necessary constraint upon burst duration (τ_a) is:

$$\tau_a \leq \text{RTLT}$$

Since the next decade of funded and proposed deep space missions will involve maximum distances to either Jupiter (Galileo Mission, International Solar Polar Mission) or Saturn (Saturn Orbiter Mission), it is immediately apparent from Fig. 18 that one is constrained with this technique to search for waves in which the amplitude is $\sim 10^{-15}$ or less. It is also obvious that one would like to search for waves with amplitudes as low as 10^{-17}(τ_a= 40 seconds). This then motivates the selection of a "baseline" experiment to look for the strongest expected waves, and a "desirable" experiment to search for a wider variety of waves. Using this rationale, and noting that there are stringent requirements throughout the entire measurement system, consisting of:

(1) Ground tracking system

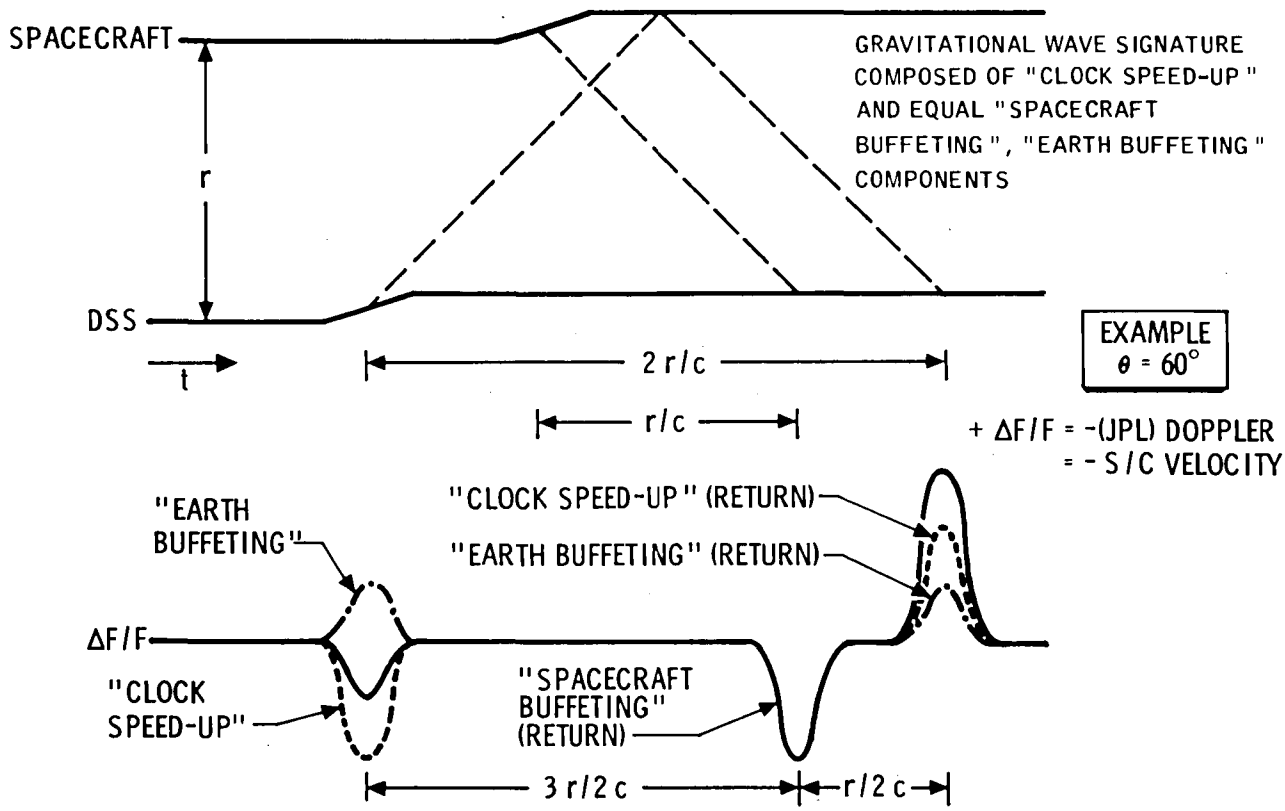

Figure 22. Unique Gravitational Wave Signature in Ultraprecise Doppler Data

(2) Transmission media

(3) Spacecraft

(4) Data processing

one proceeds to define a baseline experiment as follows:

(1) Search for waves with amplitude $h \geq 10^{-15}$.

(2) Require total measurement system fractional frequency fluctuation (σ (Δ F/F)) of 10^{-15} or less.

(3) Require each identifiable independent element of the total measurement system to have a fractional frequency fluctuation of 3×10^{-16} or less.

(4) Require averaging times (τ_a) between 50 and 5000 seconds.

Similarly, one defines a desirable experiment as follows:

(1) Search for waves with amplitudes $h \geq 10^{-17}$.

(2) Require total measurement system fractional frequency fluctuation (σ (Δ F/F)) of 10^{-17} or less.

(3) Require each identifiable independent element of the total measurement system to have a fractional frequency fluctuation of 3×10^{-18} or less.

(4) Require averaging times (τ_a) between 5 and 5000 seconds.

While it is considered technologically possible to achieve the baseline system in the 1980s, the desirable system may not be achieveable until the 1990s, if then.

The central element of the Tracking System is obviously the frequency standard of the FTS. The performance of the new Hydrogen Masers currently being implemented is considered to be:

$$\sigma(\Delta F/F) \simeq 3 \times 10^{-15}$$

$$\tau_a = 100 \text{ seconds}$$

so that a decrease of about an order of magnitude will be required to achieve the baseline experiment:

$$\sigma(\Delta F/F) = 3 \times 10^{-16}$$

$$50 \text{ seconds} \leq \tau_a \leq 5000 \text{ seconds}$$

Very recently, Hydrogen Maser measurements (R. L. Sydnor, private communication) have been reported at approximately the 3×10^{-16} level, through application of stringent environmental control.

Numerous other Tracking System elements will have to be evaluated as to their current performance, and the technology developed to obtain the desired frequency stability. These elements are listed in Table III.

The other major areas of work required to reach the baseline capability are concerned with the transmission media. With the current S-band (uplink)/X-band (downlink) system, one achieves a fractional frequency fluctuation of $\sim 1 \times 10^{-13}$ (Berman, 1978b). The DSN is currently planning on implementing a full X-band system (both uplink and downlink), which will result in a system performance of 1×10^{-14}. To achieve the required 3×10^{-16} level, it will be necessary to implement a simultaneous dual-frequency (S- and X-band) system that will allow precise dual frequency calibration of charged particle effects.

TABLE III. Required Performance Summary

Element	Baseline Experiment Requirement	Desirable Experiment Requirement
Total system, $\sigma(\Delta F/F)$	1×10^{-15}	1×10^{-17}
DSN Tracking System, $\sigma(\Delta F/F)$	1×10^{-15}	1×10^{-17}
Averaging time, seconds	$50 \leq \tau_a \leq 5000$	$5 \leq \tau_a \leq 5000$
Frequency and Timing Subsystem		
Frequency standard (H_2 Maser), $\sigma(\Delta F/F)$	3×10^{-16}	3×10^{-18}
Frequency distribution, $\sigma(\Delta F/F)$	3×10^{-16}	3×10^{-18}
Receiver-Exciter Subsystem		
Closed-loop receiver, $\sigma(\Delta \phi)$, X-band	$0.05^{o} \cdot \tau_a/50$	$0.00005^{o} \cdot \tau_a/5$
Doppler extractor, $\sigma(\Delta \phi)$, X-band	$0.05^{o} \cdot \tau_a/50$	$0.00005^{o} \cdot \tau_a/5$
Exciter, $\sigma(\Delta \phi)$, X-band	$0.05^{o} \cdot \tau_a/50$	$0.00005^{o} \cdot \tau_a/5$
Antenna Mechanical Subsystem, $\sigma(\Delta L)$	$0.005 \text{ mm} \cdot \tau_a/50$	$0.000005 \text{ mm} \cdot \tau_a/5$
Antenna Microwave Subsystem, $\sigma(\Delta \phi)$ X-band	$.05^{o} \cdot \tau_a/50$	$0.00005^{o} \cdot \tau_a/5$
Transmitter Subsystem, $\sigma(\Delta \phi)$, X-band	$0.05^{o} \cdot \tau_a/50$	$0.00005^{o} \cdot \tau_a/5$
System Cabling, $\sigma(\Delta F/F)$	3×10^{-16}	3×10^{-18}
Data processing software		
Numerical accuracy, X-band	1×10^{-4} cycle	1×10^{-7} cycle
Spacecraft		
Radio Subsystem, $\sigma(\Delta F/F)$	3×10^{-16}	3×10^{-18}

REFERENCES

Anderson, J. D., and M. R. Warner (1966), Determination of the Masses of the Moon and Venus, and the Astronomical Unit from Radio Tracking of Mariner II, Trajectories of Artificial Celestial Bodies, 216-246, Springer-Verlag, New York.

Anderson, J. D. (1974), Geodetic and Dynamical Properties of Planets, EOS 55, 515-523.

Anderson, J. D., P. B. Esposito, W. Martin, C. L. Thornton, and D. O. Muhelman (1975), Experimental Test of General Relativity Using Time-Delay Data From Mariner 6 and Mariner 7, Astrophys. J. 200, 221-233.

Anderson, J. D., M. S. W. Keesey, E. L. Lau, E. M. Standish, Jr., and X X Newhall (1978), Tests of General Relativity Using Astrometric and Radio Metric Observations of the Planets, Astronautica 5, 43-61.

Anderson, J. D., G. W. Null, E. D. Biller, S. K. Wong, W. B. Hubbard, and J. J. MacFarlane (1980), Pioneer Saturn Celestial Mechanics Experiment, Science 207, 449-453.

Berman, A. L., and J. A. Wackley (1976), Doppler Noise Considered as a Function of the Signal Path Integration of Electron Density, DSN Progress Report 42-33, 159-193. Jet Propulsion Laboratory, Pasadena, Calif.

Berman, A. L. (1978a), Solar Wind Turbulence Models Evaluated via Observations of Doppler RMS Phase Fluctuation and Spectral Broadening in the Inner Corona, DSN Progress Report 42-44, 197-202. Jet Propulsion Laboratory, Pasadena, Calif.

Berman, A. L. (1978b), Solar Wind Density Fluctuation and the Experiment to Detect Gravitational Waves in Ultraprecise Doppler Data, DSN Progress Report 42-44, 189-196. Jet Propulsion Laboratory, Pasadena, Calif.

Berman, A. L. (1979a), A Unified Observational Theory for Solar Wind Columnar Turbulence, DSN Progress Report 42-50, 124-131. Jet Propulsion Laboratory, Pasadena, Calif.

Berman, A. L. (1979b), TCI 50: DSN Telecommunications Interfaces, Solar Corona and Solar Wind Effects in Deep Space Network/Flight Project Interface Design Handbook, edited by N. A. Renzetti, Jet Propulsion Laboratory, Pasadena, Calif.

Berman, A. L., and R. Ramos (1980), Pioneer Venus Occultation Radio Science Data Generation, IEEE Trans. on Geosci. and Remote Sensing GE-18, 11-14.

Berman, A. L., J. A. Wackley, and W. H. Hietzke (1981), A Direct Comparison of Viking 2.3 GHz Signal Phase Fluctuation and Columnar Electron Density Between 2 and 160 Solar Radii, to be submitted to J. Geophys. Res.

Bird, M. K., H. Volland, C. T. Stelzried, G. S. Levy, and B. L. Seidel (1977), Faraday Rotation Transients Observed During Solar Occultation of the Helios Spacecraft, Study of Travelling Interplanetary Phenomena, 63-74, D. Reidel, Dordrecht, Holland.

Cain, D. L., J. D. Anderson, M. S. W. Keesey, T. Komarek, P. A. Laing, and E. L. Lau (1978), Test of General Relativity with Data from Viking Orbiters and Landers, Bul. Amer. Astron. Soc. 10, 396.

Cimino, J. B., C. Elachi, A. J. Kliore, D. J. McCleese, and I. R. Patel (1980), Polar Cloud Structure as Derived from the Pioneer Venus Orbiter, J. Geophys. Res. (in press).

Davies, R. W. (1974), Issues in Gravitational Wave Detection With Space Missions, in Transactions of The International Conference on Gravitational Waves and Radiations, pp. 33-45, Centre National de la Recherche Scientifique, Paris, France.

Dennison, B., G. Melnick, M. Harwit, T. Sato, C. T. Stelzried, and D. Jauncy (1978), Deflection of Polarised Radiation: Relative Phase Delay Technique, Nature 273, 33-35.

Esposito, P. B., J. D. Anderson, and A. T. Y.Ng (1978), Experimental Determination of Mercury's Mass and Oblateness, in COSPAR: Space Research, XVII, edited by M. J. Rycroft and A. C. Stickland, pp. 639-644, Pergamon Press, New York.

Eshleman, V. R., G. Fjeldbo, J. D. Anderson, A. Kliore, and R. B. Dyce (1968), Venus: Lower Atmosphere not Measured, Science 162, 661-665.

Eshleman, V. R., G. L. Tyler, J. D. Anderson, G. Fjeldbo, G. S. Levy, G. E. Wood and T. A. Croft (1977), Radio Science Investigations with Voyager, Space Science Reviews 21, 207-232.

Eshleman, V. R., G. L. Tyler, G. E. Wood, G. F. Lindal, J. D. Anderson, G. S. Levy, and T. A. Croft (1979a), Radio Science with Voyager 1 at Jupiter: Preliminary Profiles of the Atmosphere and Ionosphere, Science 204, 976-978.

Eshleman, V. R., G. L. Tyler, G. E. Wood, G. F. Lindal, J. D. Anderson, G. S. Levy, and T. A. Croft (1979b), Radio Science with Voyager at Jupiter: Initial Voyager 2 Results and a Voyager 1 Measure of the Io Torus, Science 206, 959-962.

Estabrook, F. B., and H. D. Wahlquist (1975), Response of Doppler Spacecraft Tracking to Gravitational Radiation, Gen. Rel. and Grav. 6, 439-447.

Fjeldbo, G. (1964), Bistatic Radar Methods for Studying Planetary Ionospheres and Surfaces, SU-64-025, 87 pp., Stanford Electronics Laboratories, Stanford, Calif.

Fjeldbo, G., and V. R. Eshleman (1968), The Atmosphere of Mars Analyzed by Integral Inversion of Mariner IV Occultation Data, Planet. Space Sci. 16, 1035-1059.

Fjeldbo, G., A. J. Kliore, and V. R. Eshleman (1971), The Neutral Atmosphere of Venus as Studied with the Mariner V Radio Occultation Experiments, Astron. J. 76, 123-140.

Fjeldbo, G., A. Kliore, B. Seidel, D.Sweetnam, and D. Cain (1975), The Pioneer 10 Radio Occultation Measurements of the Ionosphere of Jupiter, Astron. Astrophys. 39, 91-96.

Fjeldbo, G., A. Kliore, D. Sweetnam, P. Esposito, B. Seidel, and T. Howard (1976), The Occultation of Mariner 10 by Mercury, Icarus 29, 439-444.

Fjeldbo, G., D. Sweetnam, J. Brenkle, E. Christensen, D. Farless, J. Mehta, B. Seidel, W. Michael, Jr., A. Wallio, and M. Grossi (1977), Viking Radio Occultation Measurements of the Martian Atmosphere and Topography: Primary Mission Coverage, J. Geophys. Res. 82, 4317-4324.

Goldstein, R. M., et al. (1967), The Superior Conjunction of Mariner IV, Tech. Rpt. 32-1092, 56 pp., Jet Propulsion Laboratory, Pasadena, Calif.

Goldstein, R. M. (1969), Superior Conjunction of Pioneer 6, Science 166, 598-601.

Howard, H. T., G. L. Tyler, P. B. Esposito, J. D. Anderson, R. D. Reasenberg, I. I. Shapiro, G. Fjeldbo, A. J. Kliore, G. S. Levy, D. L. Brunn, R. Dickinson, R. E. Edelson, W. L. Martin, R. B. Postal, B. Seidel, T. T. Sesplaukis, D. L. Shirley, C. T. Stelzried, D. N. Sweetnam, G. E. Wood, A. I. Zygielbaum (1974a), Mercury: Results on Mass, Radius, Ionosphere, and Atmosphere from Mariner 10 Dual-Frequency Radio Signals, Science 185, 179-180.

Howard, H. T., G. L. Tyler, G. Fjeldbo, A. J. Kliore, G. S. Levy, D. L. Brunn, R. Dickenson, R. E. Edelson, W. L. Martin, R. B. Postal, B. Seidel, T. T. Sesplaukis, D. L. Shirley, C. T. Stelzried, D. N. Sweetnam, A. I. Zygielbaum, P. B. Esposito, J. D. Anderson, I. I. Shapiro, R. D. Reasenberg (1974b), Venus: Mass, Gravity Field, Atmosphere and Ionosphere as Measured by the Mariner 10 Dual-Frequency Radio System, Science 183, 1297-1301.

Hubbard, W. B., and J. D. Anderson (1978), Possible Flyby Measurements of Galilean Satellite Interior Structure, Icarus 33, 336-341.

Kliore, A., D. L. Cain, T. W. Hamilton (1964), Determination of Some Physical Properties of the Atmosphere of Mars from Changes in the Doppler Signal of a Spacecraft on an Earth-Occultation Trajectory, Tech. Rep. 32-674, 35 pp., Jet Propulsion Laboratory, Pasadena, Calif.

Kliore, A., D. L. Cain, G. S. Levy, V. R. Eshleman, G. Fjeldbo, and F. D. Drake (1965), Occultation Experiment: Results of the First Direct Measurement of Mar's Atmosphere and Ionosphere, Science 149, 1243-1248.

Kliore, A., G. S. Levy, D. L. Cain, G. Fjeldbo, and S. I. Rasool (1967), Atmosphere and Ionosphere of Venus from the Mariner V S-Band Radio Occultation Measurement, Science 158, 1683-1688.

Kliore, A. J., and D. L. Cain (1968), Mariner V and the Radius of Venus, J. Atmos. Sci. 25, 549-554.

Kliore, A., G. Fjeldbo, B. L. Seidel, S. I. Rasool (1969), Mariners 6 and 7: Radio Occultation Measurements of the Atmosphere of Mars, Science 166, 1393-1397.

Kliore, A. (1972a), Current Methods of Radio Occultation Data Inversion in Mathematics of Profile Inversion, NASA, TM X-62, 150, edited by L. Colin, pp. 3/2-316, National Aeronautics and Space Administration, Washington, D. C.

Kliore, A. J., D. L. Cain, G. Fjeldbo, B. L. Seidel, M. J. Sykes, and S. I. Rasool (1972b), The Atmosphere of Mars from Mariner 9 Radio Occultation Measurements, Icarus 17, 484-516.

Kliore, A. J., G. Fjeldbo, B. L. Seidel, M. J. Sykes, and P. M. Woiceshyn (1973), S Band Radio Occultation Measurements of the Atmosphere and Topography of Mars with Mariner 9: Extended Mission Coverage of Polar and Intermediate Latitudes, J. Geophys. Res. 78, 4331-4351.

Kliore, A. J., G. Fjeldbo, B. L. Seidel, D. N. Sweetnam, T. T. Sesplaukis, P. M. Woiceshyn, S. I. Rasool (1975), The Atmosphere of Io from Pioneer 10 Radio Occultation Measurements, Icarus 24, 407-410.

Kliore, A. J., and P. M. Woiceshyn (1976), Structure of the Atmosphere of Jupiter from Pioneer 10 and 11 Radio Occultation Measurements, in Jupiter, edited by T. Gehrels, pp. 216-237, Univ. of Arizona Press, Tucson, Arizona.

Kliore, A. J., C. Elachi, I. R. Patel, and J. B. Cimino (1979a), Liquid Content of the Lower Clouds of Venus as Determined from Mariner 10 Radio Occultation, Icarus 37, 51-72.

Kliore, A. J., R. Woo, J. W. Armstrong, I. R. Patel, and T. A. Croft (1979b), The Polar Ionosphere of Venus Near the Terminator from Early Pioneer Venus Orbiter Radio Occultations, Science 203, 765-768.

Kliore, A. J., I. R. Patel, A. F. Nagy, T. E. Cravens, and T. I. Gombosi (1979c), Initial Observations of the Nightside Ionosphere of Venus from Pioneer Venus Orbiter Radio Occultations, Science 205, 99-102.

Kliore, A. J., G. F. Lindal, I. R. Patel, D. N. Sweetnam, H. B. Hotz, and T. R. McDonough (1980a), Vertical Structure of the Ionosphere and Upper Neutral Atmosphere of Saturn from the Pioneer Radio Occultation, Science 207, 446-449.

Kliore, A. J., I. R. Patel, G. F. Lindal, D. N. Sweetnam, H.B. Holtz, J. H. Waite, Jr., and T. R. McDonough (1980b), Structure of the Ionosphere and Atmosphere of Saturn from Pioneer 11 Saturn Radio Occultation, J. Geophys. Res. (in press).

Kliore, A. J., and I. R. Patel (1980), Vertical Structure of the Atmosphere of Venus from Pioneer Venus Orbiter Radio Occultations, J. Geophys. Res. (in press).

Koehler, R. L. (1968), Radio Propagation Measurements of Pulsed Plasma Streams from the Sun Using Pioneer Spacecraft. J. Geophys. Res. 73, 4883-4894.

Levy, G. S., T. Sato, B. L. Seidel, C. T. Stelzried, J. E. Ohlson, W. V. T. Rusch (1969), Pioneer 6: Measurement of Transient Faraday Rotation Phenomena Observed During Solar Occultation, Science 166, 596-598.

Lindal, G. F., H. B. Hotz, D. N. Sweetnam, Z. Shippony, J. P. Brenkle, G. V. Hartsell, R. T. Spear, and W. H. Michael, Jr. (1979), Viking Radio Occultation Measurements of the Atmosphere and Topography of Mars: Data Acquired During 1 Martian Year of Tracking, J. Geophys. Res. 84, 8443-8456.

Muhleman, D. O., J. D. Anderson, P. B. Esposito, and W. L. Martin (1971), Radio Propagation Measurements of the Solar Corona and Gravitational Field: Applications to Mariner 6 and 7, in Proceeding of The Conference on Experimental Tests of Gravitation Theories, Tech. Memo. 33-499, edited by R. W. Davies, pp 92-104, Jet Propulsion Laboratory, Pasadena, Calif.

Muhleman, D. O., P. B. Esposito, and J. D. Anderson (1977), The Electron Density Profile of the Outer Corona and the Interplanetary Medium from Mariner-6 and Mariner-7 Time-Delay Measurements, Astrophys. J. 211, 943-957.

Null, G. W., J. D. Anderson, and S. K. Wong (1975), Gravity Field of Jupiter from Pioneer 11 Tracking Data, Science 188, 476-477.

Null, G. W. (1976), Gravity Field of Jupiter and Its Satellites from Pioneer 10 and Pioneer 11 Tracking Data, Astron. J. 81, 1153-1161.

Ohlson, J. E., G. S. Levy, and C. T. Stelzried (1974), A Tracking Polarimeter for Measuring Solar and Ionospheric Faraday Rotation of Signals from Deep Space Probes, IEEE Transactions on Instrumentation and Measurement IM-23, 167-177.

Reasenberg, R. D., and I. I. Shapiro (1977), Solar System Tests of General Relativity, in Experimental Gravitation, Acad. Naz. dei Lincei, Roma, Italy.

Reasenberg, R. D., I. I. Shapiro, P. E. MacNeil, R. B. Goldstein, J. C. Briedenthal, J. P. Brenkle, D. L. Cain, T. M. Kaufman, T. A. Komarek and A. I. Zygielbaum (1979), Viking Relativity Experiment: Verification of Signal Retardation by Solar Gravity, Astrophys. J. 234, L219-L221.

Reid, M. S., R. C. Clauss, D. A. Bathker, and C. T. Stelzried (1973), Low-Noise Microwave Receiving Systems in a Worldwide Network of Large Antennas, Proceedings of the IEEE, 61, 1330-1335.

Rockwell, R. S. (1978), An Empirical Spectral Bandwidth Model for Superior Conjunction, DSN Progress Rep. 42-43, 216-223.

Rusch, W. V. T., and C. T. Stelzried (1972), Net-field Polarization in a Magnetically Biased Plasma, Rad. Sci. 7, 1131-1141.

Shapiro, I. I., R. D. Reasenberg, P. E. MacNeil, R. B. Goldstein, J. P. Brenkle, D. L. Cain, T. Komarek, A. I. Zygielbaum, W. F. Cuddihy, and W. H. Michael, Jr. (1977), The Viking Relativity Experiment, J. Geophys. Res. 82, 4329-4334.

Sjogren, W. L., J. D. Anderson, R. J. Phillips, and D. W. Trask (1976), Gravity Fields, IEEE Trans. Geomag. Elect. GE-14, 172-183.

Spradlin, G. L. (1980), DSN Tracking System, Mark III-79, DSN Progress Report 42-56, 7-25. Jet Propulsion Laboratory, Pasadena, Calif.

Stelzried, C. T. (1970), A Faraday Rotation Measurement of a 13-cm Signal in the Solar Corona, Tech. Report 32-1401, 83 pp., Jet Propulsion Laboratory, Pasadena, Calif.

Stelzried, C. T., G. S. Levy, T. Sato, W. V. T. Rusch, J. E. Ohlson, K. H. Schatten and J. M. Wilcox (1970), The Quasi-Stationary Coronal Magnetic Field and Electron Density as Determined from a Faraday Rotation Experiment, Sol. Phys. 14, 440-456.

Tappan, R. W. (1974), Planetary Ranging, Tech. Rpt. 32-1526, Vol. XIX, 165-168. Jet Propulsion Laboratory, Pasadena, Calif.

Thorne, K. S. and V. B. Braginsky (1976), Gravitational-Wave Bursts from the Nuclei of Distant Galaxies and Quasars: Proposal for Detection Using Doppler Tracking of Interplanetary Spacecraft, Astrophys. J. 204, L1-L6.

Volland, H., M. K. Bird, G. S. Levy, C. T. Stelzried, and B. L. Seidel (1977), Helios-1 Faraday Rotation Experiment: Results and Interpretations of the Solar Occultations in 1975, J. Geophys. 42, 659-672.

Woo, R., F. C. Yang, K. W. Yip, and W. B. Kendall (1977), Measurements of Large-Scale Density Fluctuations in the Solar Wind Using Dual-Frequency Phase Scintillations, Astrophys. J. 210, 568-574.

Woo, R. (1978), Radial Dependance of Solar Wind Properties Deduced from Helios 1/2 and Pioneer 10/11 Radio Scattering Observations, Astrophys. J. 219, 727-739.

Woo, R., and J. W. Armstrong (1979), Spacecraft Radio Scattering Observations of the Power Spectrum of Electron Density Fluctuations in the Solar Wind, J. Geophys. Res. 84, 7288-7296.

Woo, R., J. W. Armstrong and A. Ishimaru (1980), Radio Occultation Measurements of Turbulence in The Venus Atmosphere by Pioneer Venus, J. Geophys. Res. (in press).

ABBREVIATIONS

DRA	Digital Recording Assembly
DRS	DSS Radio Science Subsystem
DSN	Deep Space Network
DSS	Deep Space Station
FTS	Frequency and Timing Subsystem
HSDL	high-speed data line
LCP	left circular polarization
MMR	Multi-Mission Open-Loop Receiver
NOCC	Network Operations Control Center
NRS	NOCC Radio Science Subsystem
OCI	operator control instruction
ODR	Original Data Record
ODA	Occultation Data Assembly
RCP	right circular polarization
RCV	Receiver-Exciter Subsystem
RTLT	round-trip-light-time
SSI	Spectral Signal Indicator
UWV	Antenna Microwave Subsystem
VCO	voltage-controlled oscillator

End of Document